Cranial Ontogeny of the Early Triassic Basal Cynodont *Galesaurus planiceps*

SANDRA C. JASINOSKI* AND FERNANDO ABDALA
Evolutionary Studies Institute, University of the Witwatersrand, Private Bag 3, WITS 2050, Johannesburg, South Africa

ABSTRACT

Ontogenetic changes in the skull and mandible of thirty-one specimens of *Galesaurus planiceps*, a basal non-mammaliaform cynodont from the Early Triassic of South Africa, are documented. The qualitative survey indicated eight changes in the craniomandibular apparatus occurred during growth, dividing the sample into three ontogenetic stages: juvenile, subadult, and adult. Changes in the temporal region, zygomatic arch, occiput, and mandible occurred during the transition from the subadult to adult stage at a basal skull length of 90 mm. At least four morphological and allometric differences divided the adult specimens into two morphs, indicating the presence of sexual dimorphism in *Galesaurus*. Differences include extensive lateral flaring of the zygomatic arches in the "male" morph resulting in a more anterior orientation of the orbits, and a narrower snout in the "female". This is the first record of sexual dimorphism in a basal cynodont, and the first time it is quantitatively documented in a non-mammaliaform cynodont. An ontogenetic comparison between *Galesaurus* and the more derived basal cynodont *Thrinaxodon* revealed differences in the timing and extent of sagittal crest development. In *Galesaurus*, the posterior sagittal crest, located behind the parietal foramen, developed relatively later in ontogeny, and the anterior sagittal crest rarely formed suggesting the anterior fibres of the temporalis were less developed than in *Thrinaxodon*. In contrast, craniomandibular features related to the masseters became more developed during the ontogeny of *Galesaurus*. The development of the adductor musculature appears to be one of the main factors influencing skull growth in these basal non-mammaliaform cynodonts. Anat Rec, 00:000–000, 2016. © 2016 Wiley Periodicals, Inc.

Key words: allometry; bivariate analysis; therapsida; skull; growth; mandible; orbit orientation; sexual dimorphism; multivariate

Galesaurus planiceps was a basal non-mammaliaform cynodont found in the Early Triassic Karoo basin of South Africa. It is characterized by distinctive sectorial postcanine teeth, which consist of a large recurved anterior cusp and a smaller posterior cusp (Rigney, 1938). *Galesaurus* was the first non-mammaliaform cynodont to be described in the literature (Owen, 1859), although it was initially classified as a member of the Crocodilia. *Galesaurus*, along with the more derived basal cynodont *Thrinaxodon liorhinus* (Fig. 1), were part of the Early Triassic recovery fauna after the end-Permian extinction

Grant sponsors: DST-NRF Centre of Excellence in Palaeosciences (CoE-Pal); National Research Foundation (NRF).

*Correspondence to: Sandra C. Jasinoski, Evolutionary Studies Institute, University of the Witwatersrand, Private Bag 3, WITS 2050, Johannesburg, South Africa. Fax: +27-11-717-6684. E-mail: sandra_jas@hotmail.com

Received 27 November 2015; Revised 20 June 2016; Accepted 22 June 2016.

DOI 10.1002/ar.23473
Published online 00 Month 2016 in Wiley Online Library (wileyonlinelibrary.com).

event, appearing soon after the Permo-Triassic boundary (Smith and Botha, 2005; Smith and Botha-Brink, 2014). A recent study of the cranial ontogeny of *Thrinaxodon* (Jasinoski et al., 2015) indicated that an ontogenetic analysis of other basal cynodonts such as *Galesaurus* is required so that the cranial morphological changes could be put into a larger phylogenetic context.

The holotype of *Galesaurus planiceps* (NHMUK 36220), consisting only of a skull and mandible, was first described by Owen (1859, 1860) and further description was undertaken by Owen (1876) and Watson (1920). Most of the subsequent comprehensive studies of the cranial morphology of *Galesaurus* were done prior to the 1940s (e.g., Broom, 1932a; Parrington, 1934; Rigney, 1938). The more recent cranial descriptions of *Galesaurus* include studies by Brink (1965), van Heerden (1972), Abdala (2003), and Abdala and Damiani (2004), the latter being the only ontogenetic study of the skull of *Galesaurus*.

Over the years, several taxa have been synonymized with *Galesaurus planiceps* (Table 1). The taxon *Glochinodon detinens*, originally described by van Hoepen (1916), was synonymized with *Galesaurus* by Broom (1932a,b). Hopson and Kitching (1972) synonymized *Glochinodontoides gracilis* (Haughton, 1924) and *Notictosaurus trigonocephalus* (Brink and Kitching, 1951) with *Galesaurus* (Table 1). *Notictosaurus* had a narrow, triangular-shaped skull; hence the species name *N. trigonocephalus* (Brink and Kitching, 1951). On the contrary, specimens previously assigned to *Glochinodontoides* were characterized by a wide skull with extensively flared zygomatic arches (pers. obs.).

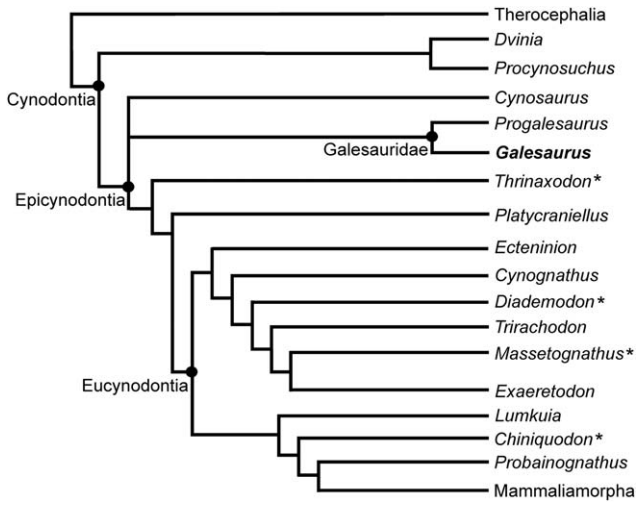

Fig. 1. Cladogram of Cynodontia showing the relationships among the epicynodonts and the more derived non-mammaliaform eucynodonts (modified from Abdala [2007: fig. 9]). Cynodont taxa included in previous allometric studies are marked with an asterisk (*).

A recent study of the postcrania by Butler (2009) determined that the *Galesaurus* sample can be divided into gracile and robust morphs, with differences manifesting in the girdle and upper limb bones. The larger specimens of *Galesaurus* (≥90% of maximum adult size in her sample) were classified as belonging to the robust type (Butler, 2009: table 3). It could not be determined whether these two morphological groups were due to sexual dimorphism, ontogeny, or different subspecies (Butler, 2009). This division between small and large specimens of *Galesaurus* was recognized historically, with small specimens commonly assigned to *Galesaurus* (including the synonymized *Glochinodon detinens*) and large specimens assigned to *Glochinodontoides* (see review by Hopson and Kitching, 1972; Table 1).

Here we describe changes in skull morphology across a large sample of *Galesaurus* using an allometric study and a qualitative comparative analysis. The latter analysis includes gross morphology and data from micro-computed tomography (micro-CT) to investigate the internal morphology of the skull. Differences among individuals of *Galesaurus* are assessed by considering ontogenetic growth, individual variation, and/or sexual dimorphism. In addition, comparisons of skull growth and function between *Galesaurus* and *Thrinaxodon* are undertaken.

MATERIALS AND METHODS

Gross Anatomical Specimens

Thirty-one specimens of *Galesaurus planiceps*, ranging in size from 54 to 114 mm of basal skull length (BSL), were included in this survey (Fig. 2; Table 2). The two smallest specimens of *Galesaurus* (BP/1/2513B,C; Table 2) were associated with a much larger individual (BP/1/2513A), and have been interpreted to represent the juvenile and adult stages, respectively (Brink, 1965). The majority of *Galesaurus* specimens have been mechanically prepared and the mandible is in situ, which makes it difficult to observe the dorsolateral part of the coronoid process. However, specimen SAM-PK-K1119 had been acid-prepared and the mandible was detached from the skull. To observe the suture morphology on the cranial surface (=ectocranial trace), acetone and/or

TABLE 1. Specimens of *Galesaurus planiceps* that were previously identified under other names

Previous identification	Specimen number	Holotype	Reference
Glochinodon detinens	TM 24	Yes	van Hoepen, 1916
Glochinodontoides gracilis	TM 83	Yes	Haughton, 1924
Glochinodontoides gracilis	AMNH 2223		Boonstra, 1935
Glochinodontoides gracilis	NMQR 1451 (NM C.1186)		Brink, 1954b
Notictosaurus trigonocephalus	BP/1/2513A (478, 223)	Yes	Brink and Kitching, 1951
Notictosaurus luckhoffi[a]	BP/1/3892		Brink, 1965
Notictosaurus luckhoffi[a]	BP/1/2513B,C (373)		Brink, 1965
Platycraniellus elegans[b]	NMQR 860 (NM C.476)		Brink, 1954a

[a]Note that the holotype of *Notictosaurus luckhoffi* is RC 107 (Broom, 1936), which is a subadult specimen of *Thrinaxodon liorhinus* (see Jasinoski et al., 2015). Brink (1965) synonymized *N. trigonocephalus* with *N. luckhoffi*.
[b]*P. elegans* is a valid taxon, but specimen NMQR 860 was re-identified as *G. planiceps* by Hopson and Kitching (1972).

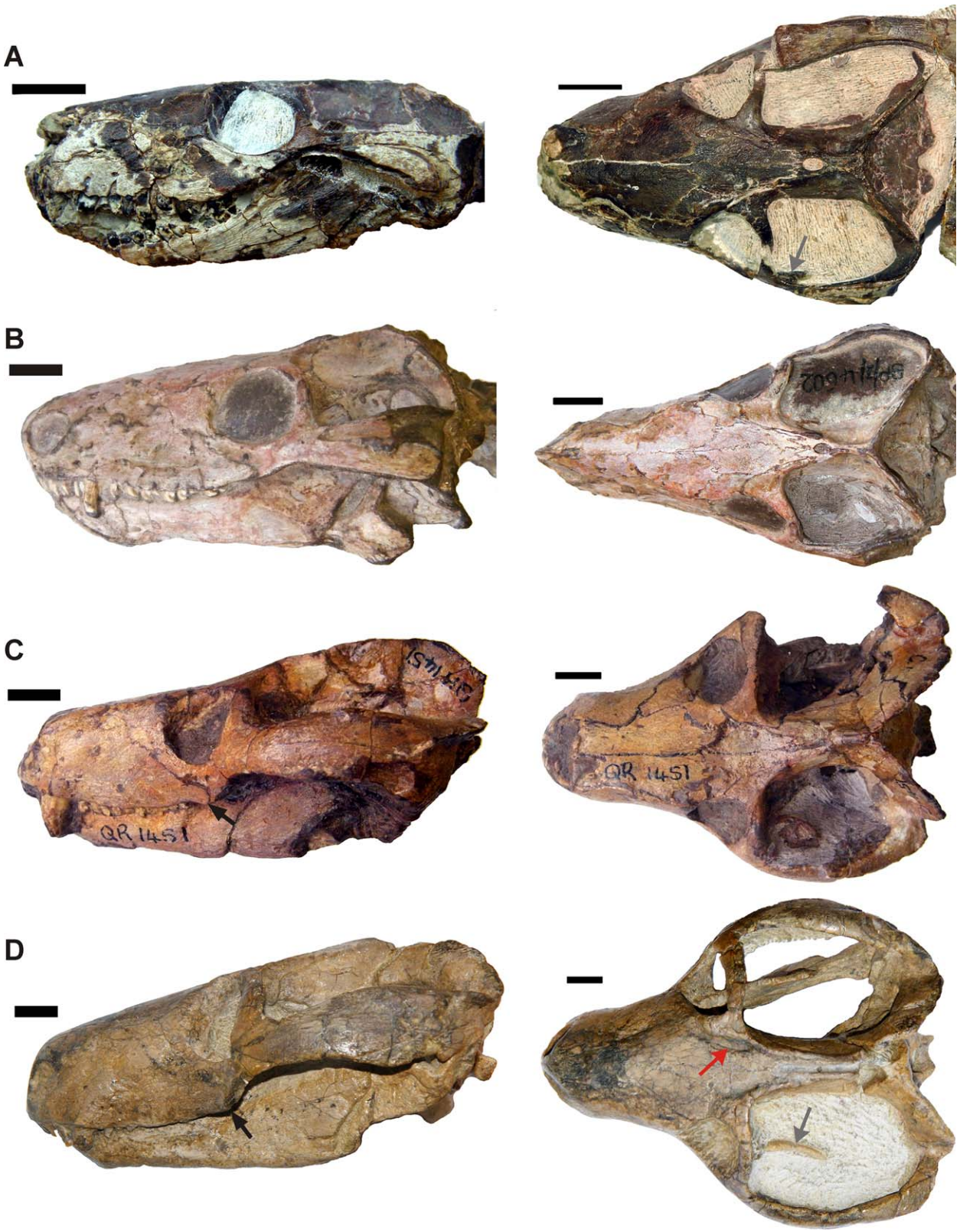

Fig. 2. Specimens of *Galesaurus planiceps* included in the present study showing the large variation in cranial shape with an increase in skull size. (**A**) NMP 581; (**B**) BP/1/4602; (**C**) NMQR 1451; (**D**) NMQR 860 (lateral image is mirrored). Left column shows the skulls in lateral view, right column is in dorsal view. In (C) and (D), the black arrow points to the angulation of the zygomatic arch. The red arrow in (D) points to the frontal parasagittal depression. Grey arrows in (A) and (D) indicate the coronoid process; note the left hemimandible is displaced posteriorly and ventrally in (A). Scale bars are 1 cm.

TABLE 2. Specimens of *Galesaurus planiceps* included in the cranial ontogenetic study

Specimen	BSL (mm)	District in South Africa	Observations
BP/1/2513C	54	Burgersdorp	Only ventral side of skull exposed
BP/1/2513B	59	Burgersdorp	
FMNH PR 1774[a,b]	62[a]	Bethulie	Serial-sectioned (Rigney, 1938)
NMP 581	64	unknown	
SAM-PK-K10465	67	Bethulie	
RC 845	69	Bethulie	Micro-CT scanned
BP/1/4597	~70	Bethulie	Eroded skull roof
TM 24	~71	Harrismith	Anterior snout missing
SAM-PK-K1119	72	Harrismith	
SAM-PK-K9956	73	Bethulie	
NMQR 3716 (3678)	75	Bethulie	Eroded skull roof
BP/1/4637	75	Bethulie	
NMQR 655	~75	Harrismith	
AMNH 2227	79	Harrismith	
SAM-PK-K8549	80	Bethulie	Mandible absent
BP/1/4714	81	Estcourt	Micro-CT scanned
UMZC T819[b]	85	Harrismith	
BP/1/4506	85	Bethulie	
BP/1/4602	88	Bethulie	Micro-CT scanned
BP/1/3892[b,c]	90[c]	Graaff-Reinet	Mandible absent
BP/1/2513A	90	Burgersdorp	
NMQR 1451	90	Bethulie	
NHMUK 36220	92	Rhenosterberg	
NMQR 135	94	Venterstad	Mandible absent; Micro-CT scanned
TM 83	94	Harrismith	
AMNH 2223	100	Harrismith	Mandible absent
NMQR 3340	~102	Dewetsdorp	Posterior skull missing
NMQR 3542	102	Bethulie	Micro-CT scanned
BP/1/5064	103	Bethulie	Eroded skull roof; Micro-CT scanned
SAM-PK-K10468	105	Bethulie	Micro-CT scanned
NMQR 860	114	Harrismith	Micro-CT scanned

Abbreviation: BSL, basal skull length.
[a]Observations taken from Rigney (1938), who incorrectly referred to the specimen as "Walker Museum 1563".
[b]Specimen not included in the bivariate and multivariate analyses.
[c]Specimen missing from collections; observations taken from Brink (1965).

water were applied to the skulls, and observations were done under a stereo microscope.

A proper diagnosis of *Galesaurus planiceps* could not be found in any of the older literature. Hopson and Kitching (1972), who synonymized three taxa with *Galesaurus* (Table 1), did not revise the genus or species diagnosis. The best description we could find is by Haughton and Brink (1954: 158–9), but it is very general and out-dated: "Skull small, fairly broad across squamosals. Snout tapering forwards. Parietal foramen large; parietal region moderately broad. Twelve upper and twelve lower post-canine teeth with two cusps, the larger of which is curved over backwards. Secondary palate complete but not well developed." Therefore, a revised diagnosis of *G. planiceps* is required but is outside of the scope of this study.

All specimens were considered to belong to *Galesaurus planiceps* based on four craniodental features: predominance of recurved bicuspid postcanines (PCs), absence of cingular and labial cusps on the PCs, absence of an interpterygoid vacuity, and an incomplete secondary palate. The maximum basal skull length in *Galesaurus* is 114 mm (Table 2). Note that PCs of at least two small specimens (BP/1/4597 [one PC on left side], NMQR 3716 [left PC5, PC6]) were found to have a small accessory cusp anterior to the main (large) recurved cusp. This variation in the postcanine dentition has not previously been recognized, and we assume here that it is related to ontogenetic development of the teeth.

The main diagnostic feature that differentiates *Galesaurus* from the contemporary basal epicynodont *Thrinaxodon liorhinus* is the distinctive morphology of the recurved bicuspid postcanines (Broom, 1932b). In addition, the maxillae that form part of the secondary palate are anteroposteriorly shorter in *Galesaurus*, the lacrimal in *Galesaurus* has an anterior process that forms a wedge between the maxilla and nasal bones, and the reflected lamina of the angular is a more rounded, dorsally expanded plate in *Galesaurus* relative to that of *Thrinaxodon*. *Platycraniellus elegans*, the other contemporary basal epicynodont (Fig. 1), does not have well-preserved teeth (Abdala, 2007); however, it can be differentiated from the large specimens of *Galesaurus* by the presence of a longer secondary palate and an interpterygoid vacuity.

To compare ontogenetic features within a broader evolutionary context, specimens of other basal epicynodonts were considered (Fig. 1). Recent ontogenetic studies of *Thrinaxodon liorhinus* (Abdala et al., 2013; Jasinoski et al, 2015) provided a useful comparison to *Galesaurus*. The contemporaneous cynodont *Thrinaxodon* was also found in the Karoo Basin, but it was much more abundant than *Galesaurus* (see Smith et al., 2012: table 2.5) and it had a longer stratigraphic range. The only

specimen of *Progalesaurus lootsbergensis* (SAM-PK-K9954; BSL 93.5 mm), the sister taxon to *Galesaurus planiceps* (Sidor and Smith, 2004; Abdala, 2007; Fig. 1), was also used as a comparison. The comprehensive description of *Progalesaurus* revealed some similarities to *Galesaurus*, including the recurved morphology of the main cusp of the postcanine teeth (Sidor and Smith, 2004). It is assumed that this galesaurid is an adult individual based on the presence of the angulation of the zygomatic arch (see Abdala and Damiani, 2004: table 1).

Serial Sections

Only a single unequivocal skull of *Galesaurus planiceps*, FMNH PR 1774 (formerly Walker Museum 1563; Rigney, 1938), has been serial-sectioned (Table 2). Rigney (1938) serially ground the small specimen (BSL 62 mm) and illustrated most of the cranial sections (intervals of 0.5 mm, but 1.0 mm intervals for the first 11 sections). Olson (1944: fig. 4A) presented a new lateral restoration of *Galesaurus* from these serial sections.

Note that the serial-sectioned AMNH FR 7600, which was apparently collected from the Permian of South Africa, was not included in this study due to a lack of specimen information and the possibility that it is not *Galesaurus*.

Micro-CT Scanned Specimens

Eight specimens of *Galesaurus* were micro-CT scanned (Table 2) at the Evolutionary Studies Institute (University of the Witwatersrand, South Africa) using a Nikon Metrology XTH 225/320 LC dual source CT system. The scanned specimens include the small specimen RC 845 (scanned with an isotropic voxel size of 42.6 μm; additional scan at 50 μm), intermediate-sized specimens BP/1/4714 (68.6 μm) and BP/1/4602 (66.7 μm), as well as larger specimens NMQR 135 (58.8 μm), NMQR 3542 (80 μm), BP/1/5064 (66 μm), SAM-PK-K10468 (71.3 μm), and NMQR 860 (74.1 μm). There was poor contrast in specimens BP/1/4714 and NMQR 860.

We compared these data with micro-CT scans of six specimens of *Thrinaxodon liorhinus*, with a BSL ranging from 37 mm to 87 mm (Jasinoski et al., 2015: table 2).

Section data were observed using ImageJ (version 1.49) and VGStudio MAX 2.2 (Volume Graphics, Germany).

Allometric Analysis

An allometric study of the skull of *Galesaurus planiceps* was undertaken, following the same methods as those for the recent comprehensive ontogenetic analysis of *Thrinaxodon liorhinus* (Jasinoski et al., 2015). Twenty-eight skulls of *Galesaurus* were analysed (Table 2). Twenty-four variables of the skull (Fig. 3) were measured using a Mitutoyo digital caliper, and a few measurements were taken from digital photos using Digimizer (version 4.2.6.0, MedCalc Software, Ostend, Belgium). All measurements were taken by F. Abdala to ensure consistency.

A bivariate analysis, comparing log-transformed cranial variables with the basal skull length (Fig. 3), was undertaken. Four of the variables (AD, PD, TP, and CCL) could not be analyzed using a bivariate analysis because of the low number of specimens that have these features visible. For example, the width of the transverse process of the pterygoids (TP) was measurable in only a few specimens due to lack of preparation and the presence of an in situ mandible; therefore only the ratio between TP and skull width (SW) was calculated.

The coefficients of allometry were calculated using the software PAST (Hammer et al., 2001). Two methods were used to calculate the coefficients: reduced major axis (RMA) and least squares (LS) (Table 3). Allometric results calculated via RMA for *Galesaurus* were then compared to the basal epicynodont *Thrinaxodon liorhinus* (Jasinoski et al., 2015), as well as three eucynodonts: the gomphodont *Diademodon tetragonus* (Grine and Hahn, 1978; Grine et al., 1978; Bradu and Grine, 1979; see also Jasinoski et al., 2015), the traversodontid *Massetognathus pascuali* (Abdala and Giannini, 2000), and the probainognathian *Chiniquodon theotonicus* (Abdala and Giannini, 2002) (Table 4).

Multivariate Analysis

We performed *a posteriori* principal component analysis (PCA) to determine if the adult sample could be further differentiated by shape and size, and explore morphological variation possibly related to sexual dimorphism. Two sets of data were analyzed. The complete set included all 20 variables and 28 specimens (Table 2) that were previously analyzed in the bivariate analysis; measurements that were missing were replaced by column average (see Hammer, 2015). The second set included 15 individuals (two juveniles, seven subadults, six adults) that have values for all nine variables (BSL, MUL, BW, OL, IO, TEL, MTO, SW, ZH). For the second data set, geometric mean was calculated for each individual and raw data were scaled by geometric mean (GM) in order to eliminate size (Mosiman and James, 1979; Meachen-Samuels and Van Valkenburgh, 2009). Both data sets were analyzed as a between group variance-covariance matrix in PAST (Hammer et al., 2001).

Institutional Abbreviations

Cynodont specimens from the following institutions were included in this comprehensive study: AMNH, American Museum of Natural History, New York, U.S.A.; BP, Evolutionary Studies Institute (formerly Bernard Price Institute for Palaeontological Research), University of the Witwatersrand, Johannesburg, South Africa; FMNH, Field Museum of Natural History, Chicago, U.S.A.; NHMUK, The Natural History Museum, London, U.K.; MCP, Museu de Ciências e Tecnologia, Pontifícia Universidade Católica do Rio Grande do Sul, Porto Alegre, Brazil; NMP, KwaZulu-Natal Museum, Pietermaritzburg, South Africa; NM or NMQR, National Museum, Bloemfontein, South Africa; PVL, Colección Paleontología de Vertebrados Lillo, Universidad Nacional de Tucumán, Argentina; RC, Rubidge Collection, Wellwood, Graaff Reinet, South Africa; SAM, Iziko South African Museum, Cape Town, South Africa; TM, Ditsong National Museum of Natural History (formerly Transvaal Museum), Pretoria, South Africa; UMZC, University Museum of Zoology, Cambridge, U.K.

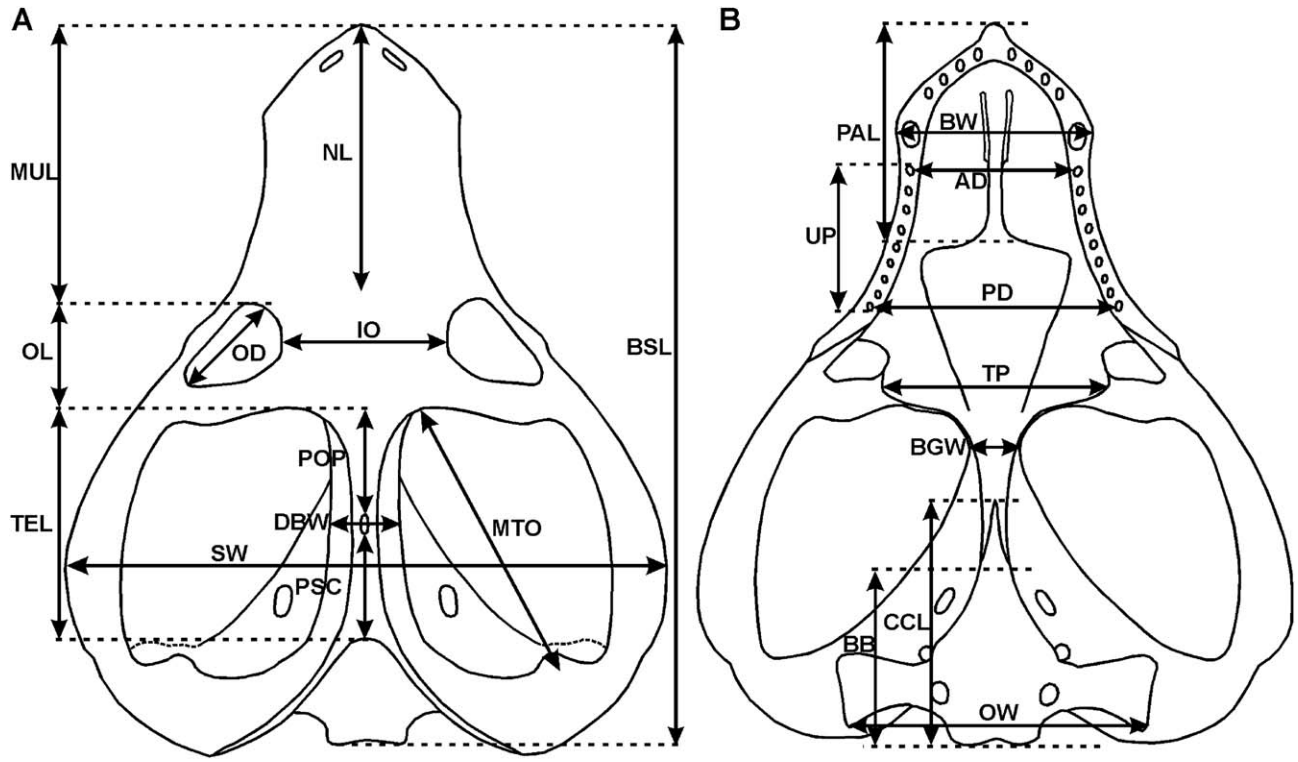

Fig. 3. Twenty-four cranial variables were measured in the skull of *Galesaurus*. (**A**) Dorsal view of an adult specimen (modified from Boonstra [1935: fig. 1]); (**B**) ventral view (modified from Boonstra [1935: fig. 2]). Abbreviations: BSL, basal skull length. Snout and palate: AD, anterior postcanine distance; BW, maxillary bicanine width; MUL, muzzle length; NL, nasal length (posterior limit defined by the nasal-frontal suture, not shown); PAL, palate length; PD, posterior postcanine distance; TP, width of the transverse process of the pterygoid; UP, upper postcanine tooth row length. Temporal region: DBW, width of the braincase in dorsal view; MTO, maximum length of the temporal opening; POP, length from postorbital bar to anterior margin of parietal foramen; PSC, length from posterior margin of parietal foramen to posterior margin of sagittal crest; TEL, temporal region length; SW, maximum skull width; ZH, maximum height of the zygomatic arch (not shown). Orbital region: IO, interorbital distance; OD, orbital diameter; OL, orbital length. Braincase: BB, basisphenoid-basioccipital length; BGW, basicranial girder width; CCL, length from condyle to anterior end of cultriform process; OH, occipital plate height (not shown); OW, occipital plate width. Note that variables AD, PD, TP, and CCL were not included in the bivariate and multivariate analyses due to the low number of specimens showing these features.

RESULTS

Allometric Analysis

Results of the bivariate analysis of allometry are listed in Table 3. Nine of the nineteen variables are not isometric under RMA. All of the variables related to the temporal region (TEL, POP, PSC, MTO) and zygomatic arches (SW, ZH) are strongly positive (Fig. 4). The highest positive values are for TEL and PSC (Table 3), which are both related to the lengthening of the temporal skull roof. In contrast, the variables OL (orbital length), BGW (basicranial girder width), and DBW (width of the braincase in dorsal view) are negative, and BB (basisphenoid-basioccipital length) is negative using the method of least squares (Table 3). As for the orbit, OL is negatively allometric (but note that R^2 [adjusted coefficient of determination] is low, indicating a poor fit of the values to the slope line); whereas the orbital diameter (OD) is isometric with a strong R^2 value (Table 3).

The R^2 value is <0.7 in five cases, and very low (<0.5) in two of these cases, both which show negative allometry (OL, BGW; Table 3). These low R^2 values may indicate that deformation of the skull affected the measurement, but they might also be an artifact of measurements that have low numerical values and therefore prone to increased instrumental error (F. Abdala, pers. obs.). This latter observation seems to explain the low R^2 values in BGW and DBW, both which are relatively small measurements.

Qualitative Differences during Ontogeny

Snout and palate.

Nasal-frontal suture. On the dorsal surface of the snout, the nasal-frontal suture is an inverted V-shape in all specimens of *Galesaurus*, including the small (Fig. 5A,B) and presumed adult (Fig. 5C) individuals. There is subtle difference in the ectocranial suture morphology, with some specimens having a relatively narrower anterior frontal projection (Fig. 5A,B) than in the larger specimens (Fig. 5C), but it appears that the tip of the frontal projection reaches or extends anterior to the margin of the orbit in all specimens.

Nasal-nasal suture. On the dorsal surface of the snout, the nasal-nasal suture appears relatively straight in the small specimens BP/1/2513B and NMP 581 (Fig.

TABLE 3. Summary of the regressions on the basal skull length of *Galesaurus planiceps*

Variables	n	R^2	b_{RMA}	$P\ (a = 1)$	b_{LS}	$P\ (a = 1)$	Trend
MUL	27	0.88	0.94	0.36	0.88	0.09	Iso
NL	17	0.79	0.89	0.29	0.79	0.06	Iso
PAL	12	0.9	0.96	0.66	0.91	0.36	Iso
BW	22	0.73	1.09	0.5	0.93	0.57	Iso
UP	19	0.84	0.9	0.28	0.83	0.06	Iso
OL	23	0.46	0.63	1.40E-03	0.43	1.30E-05	Neg
OD	18	0.91	1.02	0.77	0.97	0.74	Iso
IO	21	0.86	1.09	0.34	1.01	0.9	Iso
TEL	23	0.87	1.96	3.50E-06	1.83	2.50E-05	Pos
POP	19	0.82	1.82	0.0004	1.65	0.003	Pos
PSC	19	0.67	1.96	0.002	1.61	0.03	Pos
MTO	21	0.85	1.66	2.20E-04	1.53	0.001	Pos
SW	22	0.91	1.56	2.50E-05	1.49	1.00E-04	Pos
ZH	20	0.88	1.83	2.52E-05	1.72	0.0001	Pos
BB	12	0.69	0.73	0.06	0.6	0.01	Iso/Neg
BGW	11	0.45	0.55	0.009	0.37	0.001	Neg
OH	18	0.87	1.12	0.23	1.04	0.62	Iso
OW	22	0.86	0.99	0.89	0.92	0.32	Iso
DBW	19	0.58	0.59	0.0004	0.45	1.90E-05	Neg

Abbreviations: b_{LS}, coefficient of allometry calculated via least squares; b_{RMA}, coefficient of allometry calculated via reduced major axis method; Iso, isometry; n, sample size; Neg, negative allometry; Pos, positive allometry; R^2, adjusted coefficient of determination. Abbreviations for variables as in Figure 3.

5A), with one to two interdigitations occurring close to the midlength of the snout. The snout of SAM-PK-K10465 is eroded. In larger specimens (BSL $\geq$ 69 mm; Fig. 5B) this suture has a wavy appearance with small interdigitations that are more numerous, and in a few cases the interdigitations occur all along the length of the snout. However, the snout is eroded in most specimens with BSL 73–85 mm, making observations of this suture difficult. In one of the large individuals (NMQR 3340; Fig. 5C), the suture has more complex interdigitations on the surface of the snout but the interdigitations remain small.

Secondary palate. The secondary palate, comprising of the premaxillae, maxillae, and palatines, is not fully prepared in many specimens of *Galesaurus* because of an in situ mandible. The secondary palate is not fully closed in any specimen of *Galesaurus*: the maxillae and palatines are separated and the vomer is visible (Fig. 6). The width of the secondary palatal cleft is similar across all ontogenetic stages, with the anterior part of the cleft (which includes the foramen incisivum) being wider than the posterior part (Fig. 6).

Interpterygoid vacuity. None of the specimens of *Galesaurus* have an interpterygoid vacuity, including the small serial-sectioned specimen FMNH PR 1774 with a BSL of 62 mm (see Rigney, 1938: fig. 4).

Skull roof.

Frontal-parietal suture. The smallest specimens of *Galesaurus* (BSL $\leq$ 64 mm; Table 2) do not have a clear frontal-parietal suture on the surface of the skull roof. Specimen BP/1/2513B only has part of the right side preserved, and it shows that the parietal has two anterior projections just lateral to the midline, suggesting that the suture is interdigitated. The identification of the suture is dubious on the photo of the serial-sectioned FMNH PR 1774 skull (Rigney, 1938: pl. 1a) because there appears to be two frontal-parietal sutures (both which are interdigitated); whereas Rigney's (1938: fig. 1) reconstruction only shows a single interdigitated suture

TABLE 4. Allometric trends of *Galesaurus planiceps* compared with the basal cynodont *Thrinaxodon liorhinus* and three eucynodont taxa

Variable	*Galesaurus planiceps*	*Thrinaxodon liorhinus*	*Diademodon tetragonus*	*Massetognathus pascuali*	*Chiniquodon theotonicus*
MUL	Iso (0.94)	Pos (1.17)	Iso (1.01)	Neg (0.94)	Iso (1.02)
NL	Iso (0.89)	Iso (0.96)			
PAL	Iso (0.96)	Pos (1.15)	Iso (0.98)	Neg (0.83)	Pos (1.08)
BW	Iso (1.09)	Iso (1.1)	Iso (1.02)	Iso (0.99)	Pos (1.24)
UP	Iso (0.9)	Iso (0.93)	Neg (0.93)	Neg (0.83)	Iso (0.93)
OL	Neg (0.63)	Neg (0.65)		Neg (0.91)	Iso (0.97)
OD	Iso (1.02)	Neg (0.87)	Neg (0.69)	Neg (0.73)	
IO	Iso (1.09)	Iso (0.99)	Iso (0.92)	Iso (1.09)	Iso (1.09)
TEL	Pos (1.96)	Pos (1.41)		Pos (1.25)	Pos (1.12)
POP	Pos (1.82)	Pos (1.42)			
PSC	Pos (1.96)	Pos (1.49)			
MTO	Pos (1.66)	Pos (1.29)	Iso (1.10)		
SW	Pos (1.56)	Iso (0.95)	Pos (1.17)[a]	Pos (1.30)	Pos (1.12)
ZH	Pos (1.83)	Iso (1.17)	Pos (1.21)	Pos (1.37)[b]	Pos (1.24)
BB	Iso (0.73)	Iso (0.92)		Neg (0.87)	Pos (1.28)
BGW	Neg (0.55)	Iso (1.23)			
OH	Iso (1.12)	Pos (1.22)		Iso (1.01)	Iso (0.94)
OW	Iso (0.99)	Iso (0.9)	Pos (1.28)	Iso (1.12)	Iso (1.11)

Reduced major axis coefficients for *Thrinaxodon liorhinus* taken from Jasinoski et al. (2015); *Massetognathus pascuali* from Abdala and Giannini (2000); *Chiniquodon theotonicus* from Abdala and Giannini (2002). Jasinoski et al. (2015) used data from Bradu and Grine (1979) to calculate reduced major axis coefficients for *Diademodon tetragonus*.

[a]Marginally significant ($p = 0.07$).

[b]Result from the re-analysis of data of Abdala and Giannini (2000) (see Jasinoski et al., 2015).

Abbreviations: Iso, isometry; Neg, negative allometry; Pos, positive allometry.

Abbreviations for variables as in Figure 3.

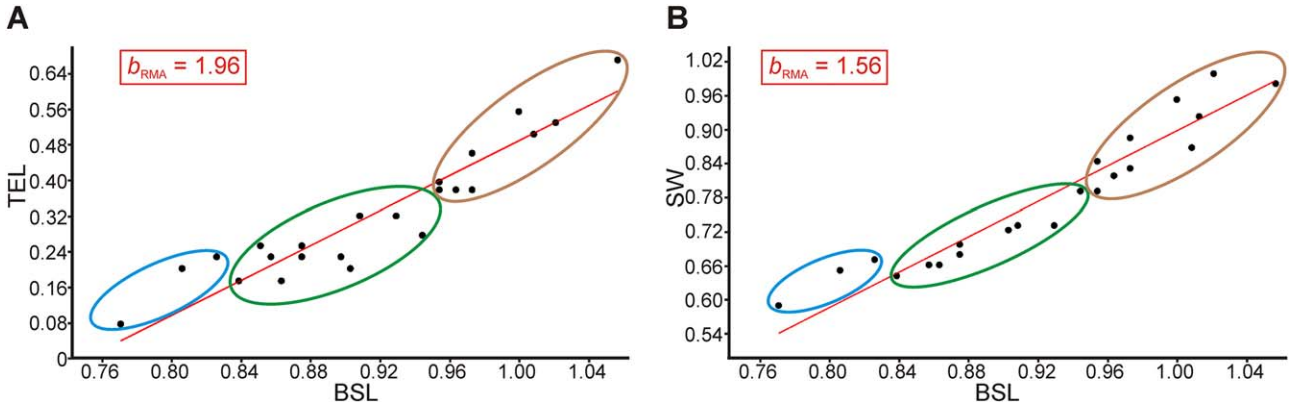

Fig. 4. Bivariate graphs (log-transformed) of *Galesaurus*. (**A**) TEL versus BSL showing strong positive allometry. (**B**) SW versus BSL showing strong positive allometry. On both graphs, the inset is the coefficient of allometry calculated via reduced major axis method, and the coloured ovals demarcate the three ontogenetic stages of *Galesaurus* (blue: juveniles; green: subadults; brown: adults). Abbreviations: BSL, basal skull length; SW, maximum skull width; TEL, temporal region length.

situated close to the parietal foramen. The suture in specimen NMP 581 is interdigitated, with two to three anterior projections occurring near the midline. In some of the larger specimens of *Galesaurus* (BSL $\geq$69 mm; e.g., RC 845, TM 24, BP/1/4602), the frontal-parietal suture near the midline of the skull is also interdigitated but it roughly forms a M-shaped morphology, with a midline frontal interdigitation that projects posteriorly followed by an anterior-projecting parietal interdigitation(s). However, this suture is not clear in most of the other large specimens because of lack of preparation, distortion, or erosion of this area.

Frontal parasagittal depressions. In three *Galesaurus* specimens larger than 102 mm BSL (NMQR 3340, NMQR 3542, NMQR 860; Table 2), the frontal bones, close to their contact with the postorbital bone on the skull roof, are characterized by distinct, paired oval-shaped depressions (Fig. 2D). However, in one large specimen (SAM-PK-K10468; BSL 105 mm), the surface of the frontal bone is shallowly depressed but does not form an oval-shaped depression.

Posterior projection of the postorbital. The posterior projection of the postorbital, which extends along the lateral edge of the skull roof, is comprised of two processes. In the small specimens (BSL$\leq$67 mm), the ventral process is much longer than the dorsal process (note that the ventral process is not visible in SAM-PK-K10465 but the dorsal process is quite short). In larger

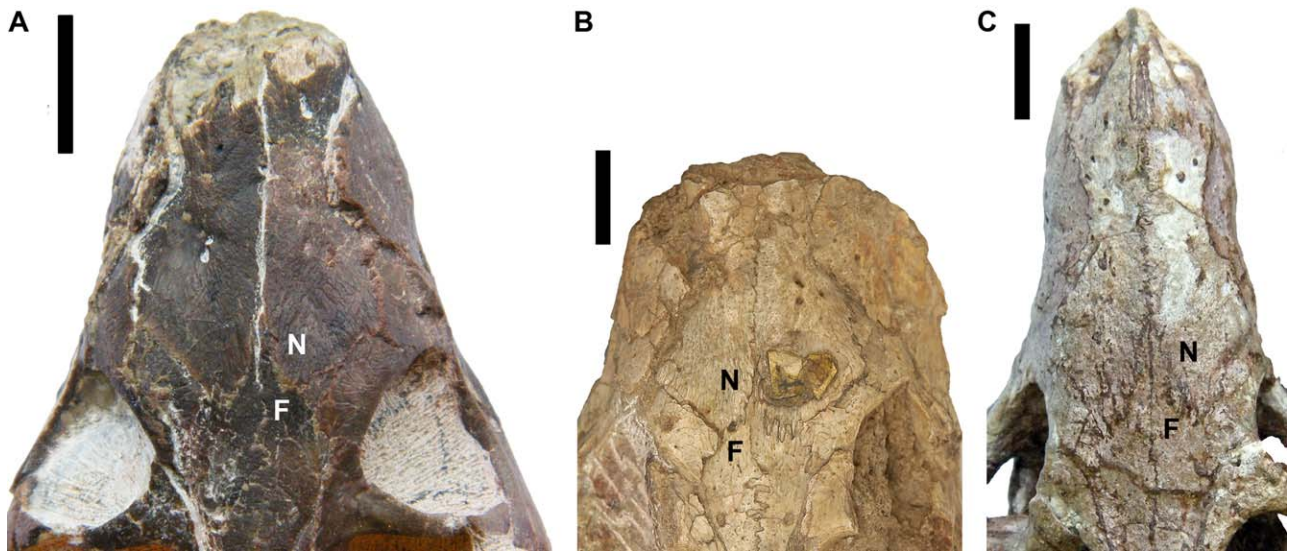

Fig. 5. Sutures on the dorsal surface of the snout of *Galesaurus*. (**A**) Juvenile specimen NMP 581 with a relatively straight nasal-nasal suture. (**B**) Subadult specimen TM 24 with an inverted V-shaped nasal-frontal suture and small interdigitations on the nasal-nasal suture. (**C**) Adult specimen NMQR 3340 with an inverted V-shaped nasal-frontal suture and a complexly interdigitated nasal-nasal suture. Abbreviations: F, frontal; N, nasal. Scale bars are 1 cm.

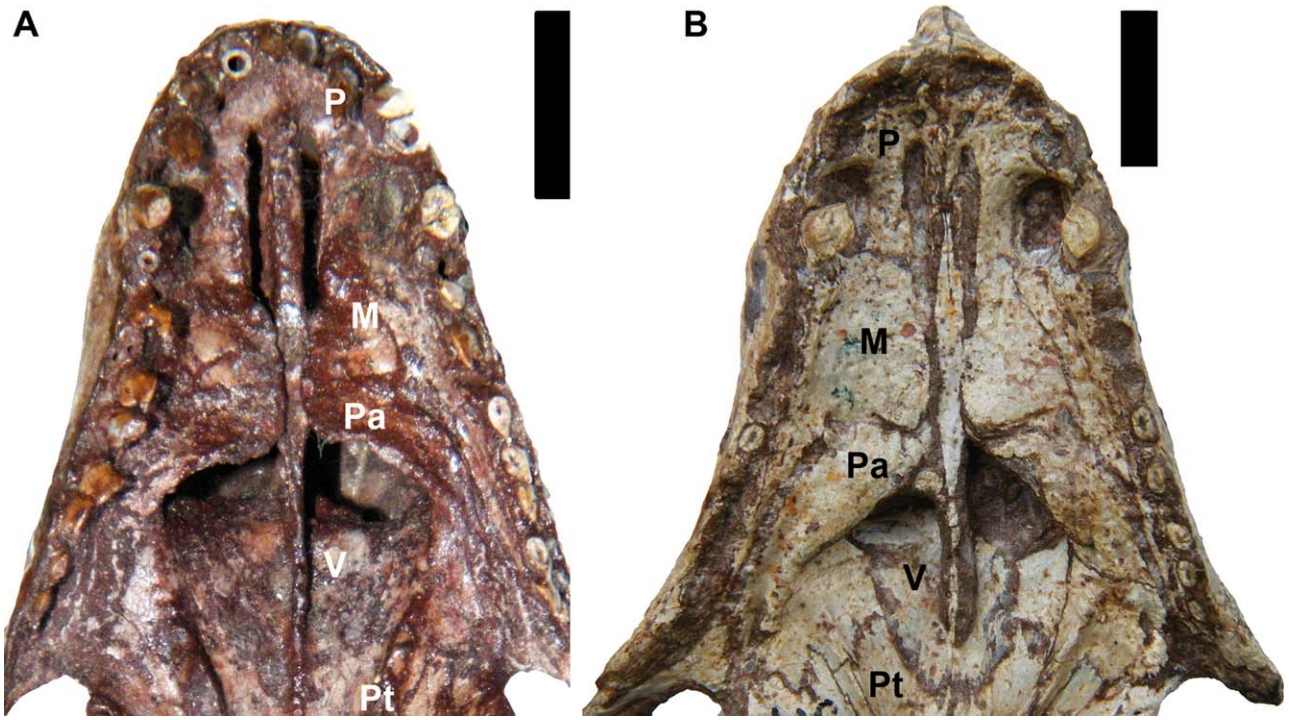

Fig. 6. Secondary palate of *Galesaurus*. (**A**) Subadult SAM-PK-K1119. (**B**) Adult NMQR 135. Abbreviations: M, maxilla, P, premaxilla, Pa, palatine; Pt, pterygoid; V, vomer. Scale bars are 1 cm.

specimens (BSL $\geq$ 69 mm), the dorsal process is subequal in length to the ventral process, forming a C-shaped (forked) projection (Fig. 2B). There is variation in the length of the posterior projection of the postorbital relative to the parietal foramen, which does not appear to be related to ontogenetic size. The largest *Galesaurus* specimen NMQR 860 was illustrated as having only a dorsal process (Abdala, 2007: fig. 7B), although re-examination revealed a slight groove for the broken ventral process on the lateral side of the skull roof. In addition, the illustration of AMNH 2223 that shows only a ventral process (Boonstra, 1935: fig. 3) is also incorrect.

Sagittal crest development. In *Galesaurus*, a sagittal crest posterior to the parietal foramen developed only in large specimens (Fig. 2, 7). As in *Thrinaxodon*, the posterior sagittal crest is formed by the coalescence of the sharp temporal ridges (see Jasinoski et al., 2015). In one of the smallest known specimens of *Galesaurus* (BP/1/2513B), there is only a faint trace of the temporal ridges posterior to the parietal foramen, which appears to be a result of over-preparation and/or erosion of the skull. The smallest well-preserved specimen, NMP 581, has a narrowed posterior sagittal table with prominent lateral temporal ridges. Specimens of intermediate size

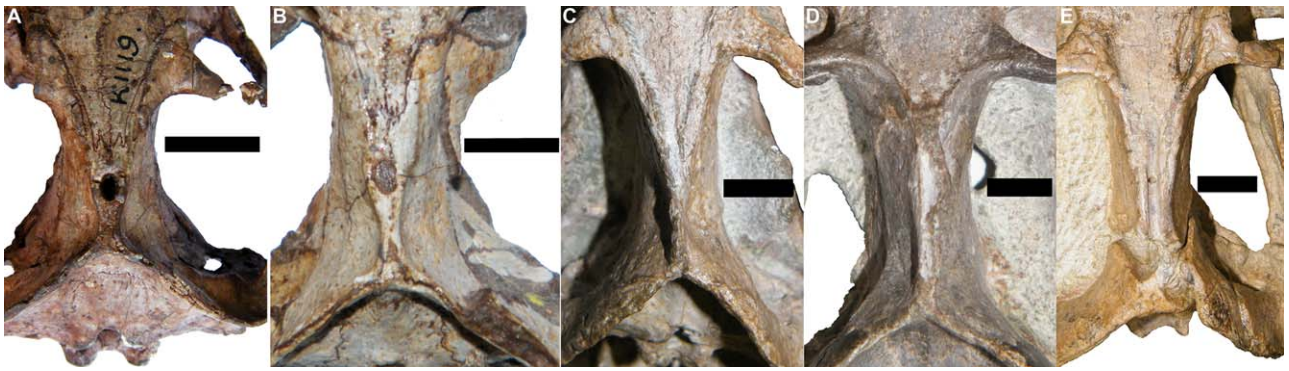

Fig. 7. Development of the posterior sagittal crest in *Galesaurus*. (**A**) SAM-PK-K1119, a subadult specimen with a posterior sagittal table. (**B**) The posterior sagittal crest developed in larger specimens with a BSL $\geq$ 88 mm (NMQR 135). (**C**) NMQR 3542 showing a well-developed posterior sagittal crest. (**D**) SAM-PK-K10468, the second largest individual of *Galesaurus*, is the only specimen with an anterior sagittal crest. (**E**) NMQR 860, the largest known specimen of *Galesaurus*, has an eroded and/or overprepared temporal region (also see Fig. 8D). Scale bars are 1 cm.

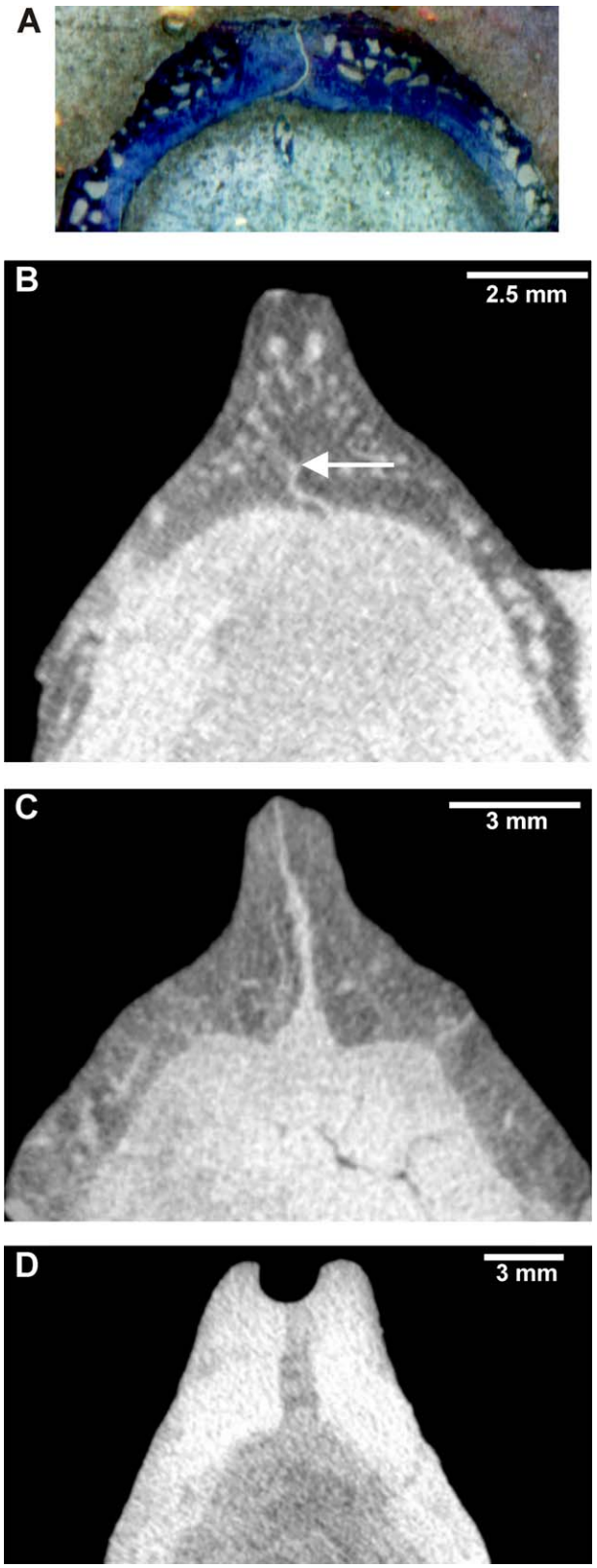

Fig. 8.

also have a posterior sagittal table (Fig. 7A). The smallest individual that has a fully developed posterior sagittal crest, with coalesced temporal ridges, is specimen BP/1/4602 (BSL of 88 mm; Fig. 2B). The height of the posterior intertemporal region, which includes both the posterior sagittal crest and the lambdoidal crest, appears to have increased with skull size (Fig. 2).

The anterior sagittal crest, however, is absent in the majority of *Galesaurus* specimens observed, and the temporal ridges form a broad, V-shaped region in dorsal view (Fig. 7A–C). There is only one specimen that unequivocally developed an anterior sagittal crest (SAM-PK-K10468; Table 2; Fig. 7D). In this large specimen, the anterior sagittal crest is taller than the corresponding broad anterior temporal region in the other large specimens.

There are two large *Galesaurus* specimens (AMNH 2223, NMQR 860; Table 2; Fig. 7E) that have a distinctively different intertemporal morphology than the other large specimens. In these specimens, the broad temporal ridges do not appear to coalesce to form a unified sagittal crest, but instead the ridges are parallel to form what appears to be a bilaminar crest separated by a median trough (Figs. 2D and 7E). However, the historical descriptions and reconstructions of NMQR 860 (Brink, 1954a: fig. 1B) and AMNH 2223 (Boonstra, 1935: fig. 1) indicate that the sagittal crest was unified and broad, without a sagittal trough. Observations of NMQR 860 under a stereo microscope revealed that the dorsal bone surface of the temporal ridges had been removed (perhaps the result of overpreparation) or was eroded, which artificially created the dorsally-flattened ridges. Further investigation of NMQR 860 using micro-CT corroborated this observation, including evidence that the dorsomedial edges of the temporal ridges are incomplete and the median trough is an artifact (Fig. 8D). The micro-CT data also indicated that the parietal-parietal suture, both anterior and posterior to the parietal foramen, was taphonomically separated (Fig. 8D); therefore in life the temporal ridges would have been positioned slightly closer together (although it is uncertain if they formed a united sagittal crest). It is not known if specimen AMNH 2223 was also affected by taphonomic processes and/or overpreparation; further investigation of this specimen using CT-scanning is necessary.

Parietal foramen. In most specimens of *Galesaurus*, the parietal foramen is oval-shaped, being anteropos

Fig. 8. Coronal sections through the skull roof of *Galesaurus* showing the posterior parietal-parietal suture (A, serial section; B-D, micro-CT sections). (**A**) The posterior parietal-parietal suture is present across the thickness of the skull roof in the juvenile specimen FMNH PR 1774 (nitrocellulose peel of section 19; compare with Rigney, 1938: pl. 3, sections 15, 18). Image courtesy of K. Angielczyk. (**B**) In the large subadult specimen BP/1/4602, which has a posterior sagittal crest, bone was deposited dorsally to the posterior parietal-parietal suture. The suture is visible only near the ventral edge of the parietal bones (white arrow marks its dorsal extent). (**C**) The condition of the posterior parietal-parietal suture in the adult specimen NMQR 135 is equivocal: the suture, located ventrally, might have continued dorsally to the ectocranial edge of the parietal bone or a crack might have formed dorsally. (**D**) In the largest specimen NMQR 860, the parietal bones have been taphonomically separated (perhaps along the midline of the suture), the temporal ridges are eroded dorsally, and the median trough is an artifact.

teriorly longer than wide. It appears to have become slightly narrower in some larger specimens, but poor preservation makes it difficult to quantify this difference. In the large specimens NMQR 3542, SAM-PK-K10468, and NMQR 860 (Fig. 7C–E), it was necessary to use micro-CT to locate the parietal foramen because it was not obvious on the surface of the skull. The micro-CT scans revealed that the parietal foramen did not disappear in these large specimens. In addition, the position of the parietal foramen in specimen NMQR 860 was found to coincide partially with the 'hole' in the skull roof, but it is longer posteriorly (Fig. 7E) (note it is located further posterior than illustrated in Abdala [2007: fig. 7A]).

Parietal-parietal suture. The condition of the parietal-parietal suture posterior to the parietal foramen in *Galesaurus* is variable, and in some cases it is not easily determined due to poor preservation and resolution of the micro-CT scans. The serial sections drawn by Rigney (1938: pl. 2 and 3, sections 13, 15, 18) and the nitrocellulose peels (Fig. 8A) show that the suture is patent across the entire depth of the skull roof in the small specimen FMNH PR 1774 (BSL 62 mm). Specimens NMP 581 and SAM-PK-K10465 have an eroded skull roof surface, and the posterior parietal-parietal suture is not visible. In specimens with a BSL ranging from 69 to 81 mm (Table 2), the presence of the suture on the surface of the skull is variable, with only three specimens (RC 845, AMNH 2227, and SAM-PK-K1119) showing dorsal obliteration of the suture. In specimen RC 845, there is no indication of a suture on the dorsal surface of the skull roof (Fig. 9A) or in the coronal micro-CT sections, but the latter have poor resolution. In the slightly larger specimen TM 24 (BSL ~71 mm; Fig. 9B), the posterior parietal-parietal suture is clearly visible ectocranially, and the suture slightly deviates to the right of the skull roof midline near the parietal foramen. The posterior parietal-parietal suture is not visible on the surface of the skull of SAM-PK-K1119 (BSL 72 mm) but an irregular ridge of bone is instead visible along the midline of the intertemporal roof, which was presumably deposited over the suture. Specimen SAM-PK-K9956 (BSL 73 mm; Fig. 9C) also has a slight ridge of bone near the midline, but there is a stippled (non-continuous) line to the right of the midline that could represent either a partially obliterated suture or a crack (micro-CT is required). In specimen NMQR 655 (BSL ~75 mm) the posterior parietal-parietal suture appears to be present to the left of the midline ridge. Specimen BP/1/4714 (BSL 81 mm; Fig. 9D) has a midline ridge developed posteriorly but the posterior parietal-parietal suture is visible to the far right of the midline.

In well-preserved specimens with a BSL 85–90 mm (Table 2), the posterior parietal-parietal suture is not visible ectocranially. The coronal micro-CT sections of BP/1/4602 (BSL 88 mm) indicate that the dorsal part of the parietals is united by solid bone, and the suture is visible only near the ventral edge of the parietals (Fig. 8B).

The condition of the parietal–parietal suture in specimens with BSL 92–114 mm BSL (Table 2) is equivocal: the intertemporal region is eroded or covered with matrix in five specimens, and the micro-CT scans of specimens NMQR 3542 and SAM-PK-K10468 have poor resolution. Specimen NMQR 135 is also equivocal: part of the suture appears visible on the dorsal surface (a non-continuous line is present to the right of the midline of the skull roof and it connects with the parietal-interparietal suture on the right side; Fig. 7B), but this instead might be a crack that extends from the dorsal extent of the posterior parietal-parietal suture to the ectocranial surface (Fig. 8C). The micro-CT scan of NMQR 860 shows that the dorsally-eroded parietal bones have been taphonomically separated (Fig. 8D), perhaps along the midline of the suture.

The anterior parietal–parietal suture appears to be patent through the entire depth of the skull roof in many of the small (e.g., Rigney, 1938: pl. 3, section 27) and presumed adult (e.g., NMQR 135) specimens. However, it is equivocal for most of the specimens with a BSL $\geq$ 100 mm (Table 2), as this area is not preserved or the suture is not clear either on the skull surface or in the micro-CT sections.

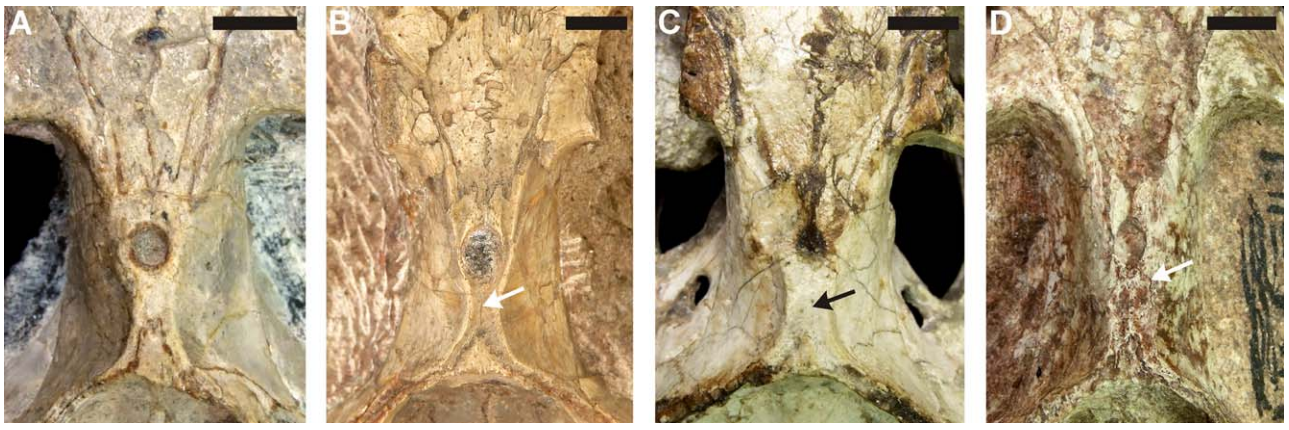

Fig. 9. Variation in the ectocranial morphology of the posterior parietal-parietal suture of *Galesaurus*. Skulls in dorsal view. The posterior parietal-parietal suture is obliterated dorsally in RC 845 (**A**); however the suture is clearly visible in TM 24 (**B**). (**C**) A partially obliterated suture or crack (black arrow) is visible in SAM-PK-K9956. (**D**) The posterior parietal-parietal suture occurs to the far right of the midline in specimen BP/1/4714. The white arrow in (B, D) points to the posterior parietal-parietal suture. Scale bars are 5 mm.

Zygoma.

Angulation of the zygomatic arch. It was noted by Abdala and Damiani (2004) and Jasinoski et al. (2015) that the zygomatic arch of larger individuals of *Galesaurus* had a suborbital angulation between the maxilla and jugal. Our survey confirms that this angulation is present in most large specimens with a BSL of 90 mm or greater (Fig. 2C,D), with the exception of specimens BP/1/2513A and TM 83.

Watson (1920: fig. 2) noted that a process on the jugal was roughened in the type specimen (NHMUK 36220), and he suggested that it indicated a scar for musculature related to the lips. After re-examination of digital photos of this poorly-preserved specimen, the jugal process described by Watson (1920) can be homologized with the angulation of the zygomatic arch, although it is apparent only on the right side of the skull.

Flaring of the zygomatic arch. In dorsal view, the zygomatic arches are straight and the outline of the skull appears triangular in small specimens of *Galesaurus* (Figs. 2A,B and 10A). The width of the zygomatic arches increased with ontogeny, as indicated by positive allometry of SW (Figs. 3A and 4B; Table 3). However in half of the larger specimens (BSL $\geq$ 90 mm; NMQR 1451, TM 83, AMNH 2223, BP/1/5064, SAM-PK-K10468, NMQR 860; Figs. 2C,D and 10B), the zygomatic arches show extensive lateral flaring, and the skull in dorsal view is much wider.

Squamosal sulcus. The squamosal sulcus is a depression on the posterolateral corner of the zygomatic arch, which is capped by a thin dorsal lip of bone. When preserved, this sulcus is shallow in most specimens of *Galesaurus*, but it is deeply developed in three large specimens (NMQR 1451, AMNH 2223, BP/1/5064; BSL $\geq$ 90 mm) (also noted by Abdala, 2003: fig. 1B). However, the large specimens NMQR 135 and NMQR 3542 only have a shallow squamosal sulcus.

Orbits.

Orbit orientation. The orientation of the orbits changed during the ontogeny of *Galesaurus*. In small specimens of *Galesaurus*, the orbits have a lateral orientation (Fig. 10A). However, in half of the presumed adult specimens (BSL $\geq$ 90 mm; NMQR 1451, TM 83, AMNH 2223, BP/1/5064, SAM-PK-K10468, NMQR 860), the orbits are oriented more anteriorly than laterally (Fig. 10B). The orbit orientation in the remaining presumed adults (BP/1/2513A, BP/1/3892 [see Brink (1965: fig. 44A)], NHMUK 36220, NMQR 135, NMQR 3340, NMQR 3542) is lateral or anterolateral.

Orbital convergence, a measure of how much the orbits face in the same direction (Cartmill, 1972), was considered in two different sized individuals of *Galesaurus*. We estimated the orientation of the orbits in a small specimen (RC 845) and the largest specimen (NMQR 860; Table 2) using a methodology similar to that of Cartmill (1972). A line approximating the orbital margin was drawn through two points on the orbit: the lacrimal-jugal suture on the anterior orbital rim and the posteroventral-most point on the orbital rim (Fig. 10). The sagittal midline of the skull was defined as the line through the interpremaxilla suture/snout tip and the middle of the parietal foramen (Fig. 10). The angle between the sagittal midline and the orbital margin line was measured to determine the approximate orientation of the orbit (Fig. 10). The angle is much lower in the small specimen (24°; Fig. 10A) compared to that of the largest specimen of *Galesaurus* (39°; Fig. 10B), indicating that the orbits face more anteriorly in the latter.

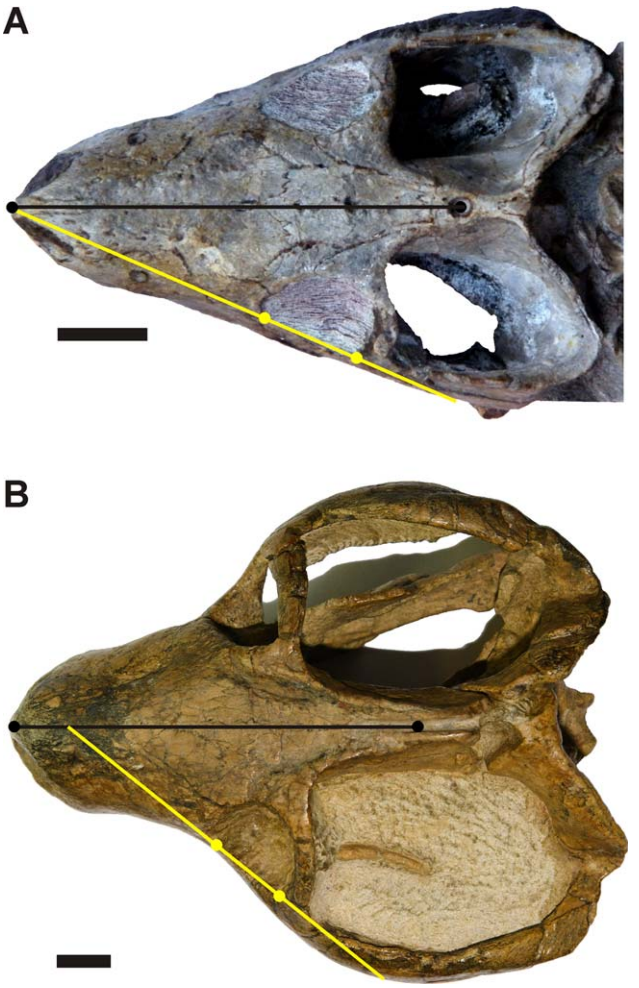

Fig. 10. Orientation of the orbits was measured in two different-sized specimens of *Galesaurus*. (**A**) Small subadult specimen RC 845 (24°); (**B**) Largest adult specimen NMQR 860 (39°). In the small subadult specimen, the zygomatic arch is not flared laterally and the outline of the skull appears triangular-shaped; whereas in the largest adult specimen, the zygomatic arch is greatly flared laterally. The orbital margin line (yellow line) was defined by the lacrimal-jugal suture on the anterior orbital rim and the posteroventral-most point on the orbital rim (yellow landmarks). The angle measured from the sagittal midline of the skull (black line) to the orbital margin line provides an estimate of the orientation of the orbits. Scale bars are 1 cm.

Basicranium.

Unossified region: basioccipital-basisphenoid. The unossified region within the basioccipital-basisphenoid bones was recognized in the micro-CT scans of specimen BP/1/4602 (Fig. 11A) (RC 845 and BP/1/4714 do not have clear micro-CT scans) and the presumed adults NMQR 135 (Fig. 11B), BP/1/5064, and SAM-PK-K10468 (NMQR 3542 has poor resolution). The largest specimen, NMQR 860 (BSL 114 mm) also appears to have an unossified

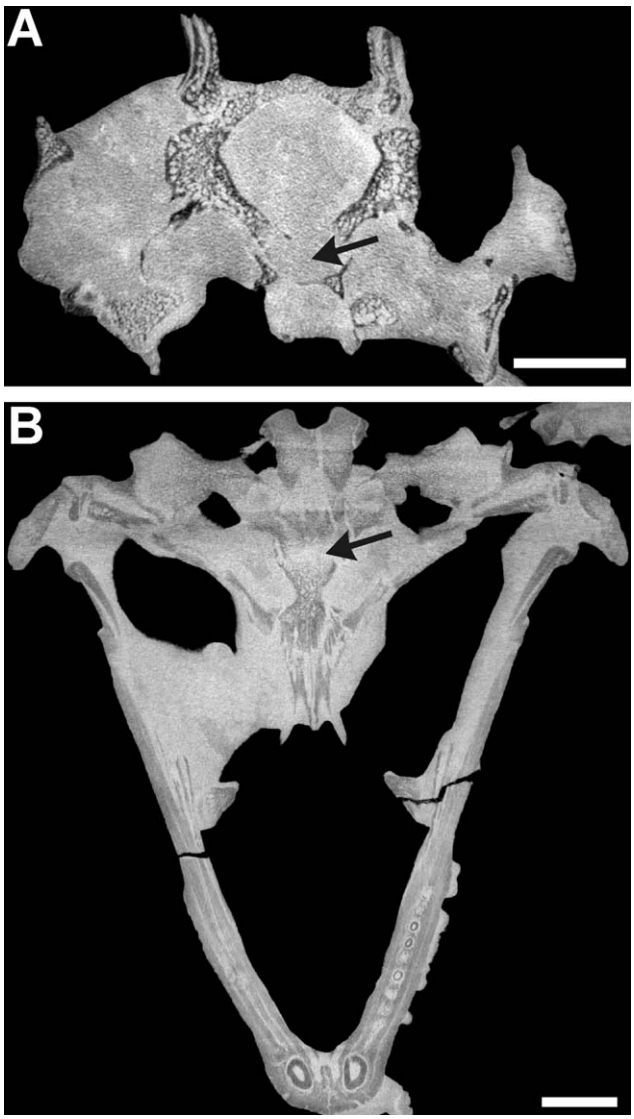

Fig. 11. Micro-CT sections through the basicranium of *Galesaurus* showing the unossified zone (arrow). (**A**) Coronal section of subadult specimen BP/1/4602; (**B**) horizontal section of the adult specimen BP/1/5064. Scale bars are 1 cm.

zone, but the micro-CT sections of the basicranial region are not as clear as in the other large specimens. Because this unossified zone is retained in the large specimens, it is assumed that the skull was still growing.

Occiput and braincase.

External occipital crest. The external occipital crest (= median nuchal line in modern mammals) is present on the interparietal and supraoccipital of the occiput in all well-preserved specimens of *Galesaurus* (Fig. 12A,C) (note that the condition in specimens with BSL $\leq$ 62 mm is not known). The external occipital crest is a rounded prominence in most specimens, but it is more ridge-like in specimen UMZC T819. In larger specimens of *Galesaurus*, the external occipital crest became more prominent and the oval-shaped fossae lateral to the crest became deeper (Table 2; Fig. 12C). These differences are non-discrete (continuous), therefore they cannot be used to divide the sample into specific size classes, but they can help to differentiate between small and large individuals.

Foramen magnum. In some *Galesaurus* specimens, the dorsolateral edge of the foramen magnum on the exoccipital has two low projections for the articulation with the proatlas. However, this feature appears to vary across specimens of different sizes without showing an ontogenetic trend.

The shape of the foramen magnum also appears to vary in *Galesaurus*. In some specimens, the foramen has a narrow dorsal notch (Fig. 12D), but in a few larger specimens the foramen magnum is more circular. It is difficult to determine if this variation is due to size differences or to intraspecific variation because the foramen magnum is often distorted or covered by postcranial elements. Because not all of the large specimens have a circular shaped foramen magnum (e.g., NMQR 1451, NMQR 135, BP/1/5064), it is assumed that the difference in shape is due to individual variation.

Fusion of exoccipital with surrounding bones. Brink (1965) noted that the sutures between the exoccipital and three surrounding occipital elements (basioccipital, opisthotic, and supraoccipital) were not demarcated in the large *Galesaurus* specimen BP/1/3892 (although these sutures are present on his fig. 44). Brink's (1954b: fig. 4A) illustration of NMQR 1451 showed that these sutures are also obliterated in this large specimen (BSL 90 mm). Our comprehensive survey also indicates that the sutures between the exoccipital and the basioccipital, opisthotic, and supraoccipital are fused in large specimens (BSL $\geq$ 90 mm; Fig. 12C,D). However, in most of the smaller specimens (BSL $<$ 90 mm; with the possible exceptions of BP/1/4714 and SAM-PK-K8549), these sutures are patent (Fig. 12A,B). It should be noted that the exoccipital-tabular suture remains patent in all ontogenetic stages (Fig. 12A,C,D).

The serial sections of the presumed juvenile specimen FMNH PR 1774 (BSL 62mm) showed that a suture is present between the exoccipital and supraoccipital and between the exoccipital and opisthotic (Rigney, 1938: pl. 2, sections 5, 6). In addition, the exoccipital and basioccipital are separate bones (Rigney, 1938: pl. 2, sections 6, 7). Therefore, this specimen agrees with our observation that the exoccipital remains separate from the surrounding bones in specimens smaller than BSL 90 mm.

However, there are two possible exceptions to this timing of fusion. In specimen BP/1/4714 (BSL 81 mm), the exoccipital–supraoccipital suture appears fused on the surface of the occiput; however it is equivocal because the micro-CT data for this area has poor contrast, and many of the other sutures on the surface of the occiput are not apparent. Specimen SAM-PK-K8549 (BSL 80 mm) has a clear suture between the supraoccipital and the tabular on the surface of the occiput, but there is no suture visible between the supraoccipital and the exoccipital as well as between the exoccipital and the opisthotic (the exoccipital-basioccipital suture is covered with matrix, and therefore its condition is unknown).

The micro-CT data for many of the presumed adult specimens indicated that the sutures are fused internally (e.g., NMQR 135), although the contrast between bones and matrix in this region was not sufficient to determine whether this was the case in all specimens (e.g., SAM-PK-K10468).

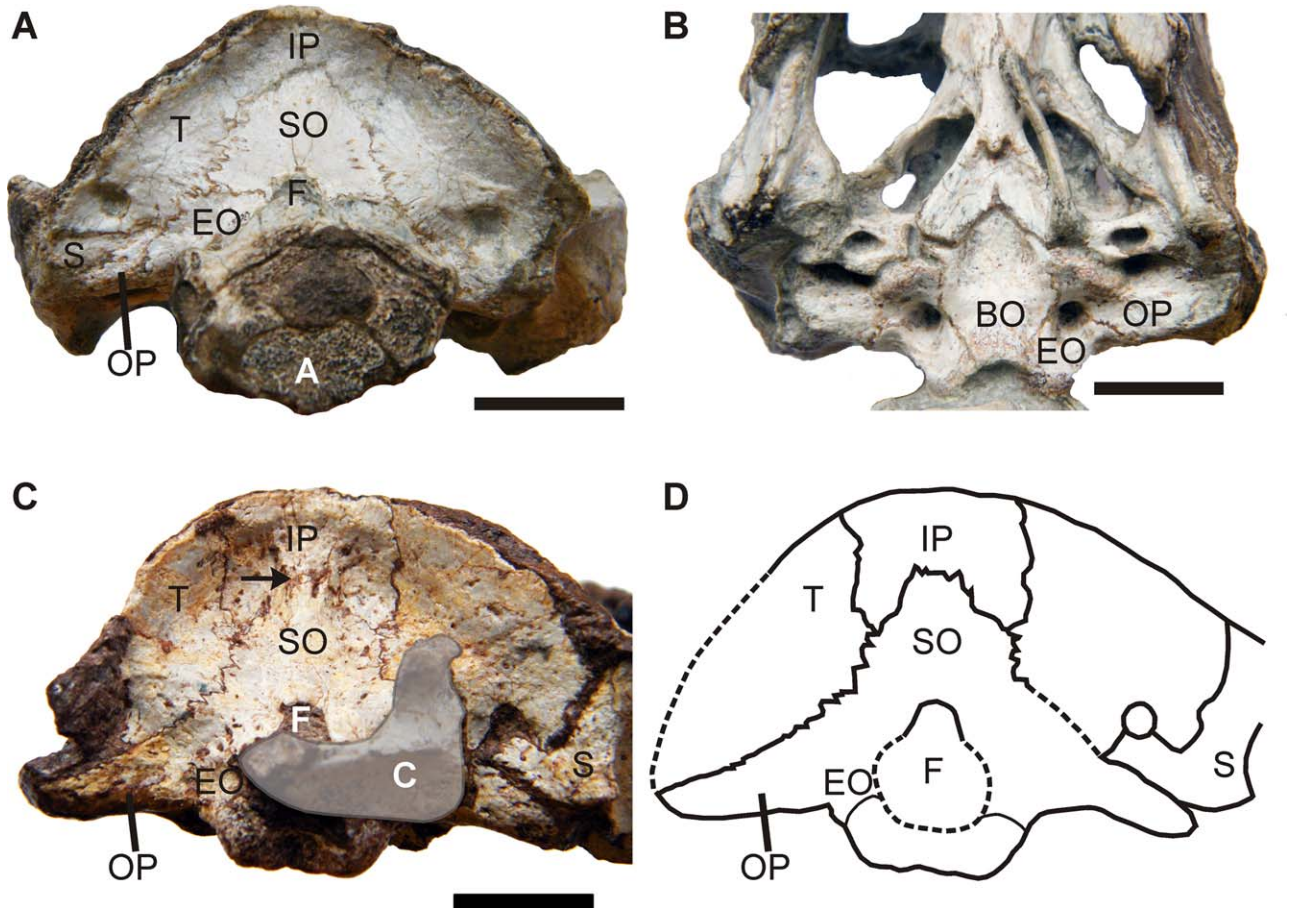

Fig. 12. The occiput (A, C, D) and basicranium (B) showing the occipital sutures in two ontogenetic stages of *Galesaurus*. (**A**) Occiput of the subadult SAM-PK-K9956 in posterior view; (**B**) ventral view of the basicranium of the subadult SAM-PK-K9956. (**C**) Occiput of the adult NMQR 135 in posterior view. Note that the left squamosal is missing and the right squamosal is displaced; costal plate is shaded in grey. Arrow indicates the external occipital crest. (**D**) Interpretive drawing of the occiput of the adult NMQR 135 showing the remaining patent sutures. Note the external occipital crest is more developed and the exoccipital is fused with three of the surrounding occipital bones (BO, OP, SO) in the adult stage (**C, D**). Abbreviations: A, atlas centrum; BO, basioccipital; C, costal plate; EO, exoccipital; F, foramen magnum; IP, interparietal; OP, opisthotic; T, tabular; S, squamosal; SO, supraoccipital. Scale bars are 1 cm.

Mandible.

Position of the mandible in the temporal fenestra. In the smaller specimens of *Galesaurus* (BSL $\leq$ 85 mm), the tip of the coronoid process and the body of the mandible are near the lateral edge of the temporal fenestra, in close proximity to the zygomatic arch (Figs. 2A and 13A,B). The relative position of the mandible became more medial with increasing age. In the larger specimens (BSL $\geq$ 88 mm; Figs. 2B–D and 13C) the tip of the coronoid process is near the middle of the temporal fenestra, leaving more space between the lateral edge of the mandible and the medial edge of the zygomatic arch than in the smaller specimens.

The repositioning of the mandible might be related to the increased lateral flaring of the zygomatic arches in large specimens (see previous section) and/or changes in the relative width of the pterygoid processes that abut against the medial edge of the mandible (Fig. 14). However, in specimen BP/1/4602, the position of the mandible is closer to the middle of the temporal fenestra but the zygomatic arches are not greatly flared (Fig. 2B). Therefore, this specimen indicates a clear influence of the width of the pterygoid processes (see Discussion for variation of the ratio between TP and SW).

Adductor fossae. The adductor fossae, situated on the posterolateral part of the dentary, include a masseteric fossa ventrally and a dorsal adductor fossa on the coronoid process. In the smaller specimens of *Galesaurus*, the masseteric fossa is not well-developed and it lacks a prominent anterior ridge that demarcates its anterior extent (Fig. 15A) (also noted by Sidor and Smith [2004] for both *Galesaurus* and *Progalesaurus*). However, in larger specimens (BSL $\geq$ 90 mm; Fig. 15B), the anterior ridge is more prominent (with the exception of SAM-PK-K10468) and the lateral swelling of the mandible is also apparent in ventral view. Interestingly, specimen NMQR 1451 (BSL 90 mm) has a low anterior ridge of the masseteric fossa on the left dentary, but it is not yet developed on the right dentary.

Compared to the masseteric fossa, the dorsal adductor fossa on the lateral side of the coronoid process appears more prominent (Fig. 15C,D). In larger specimens of

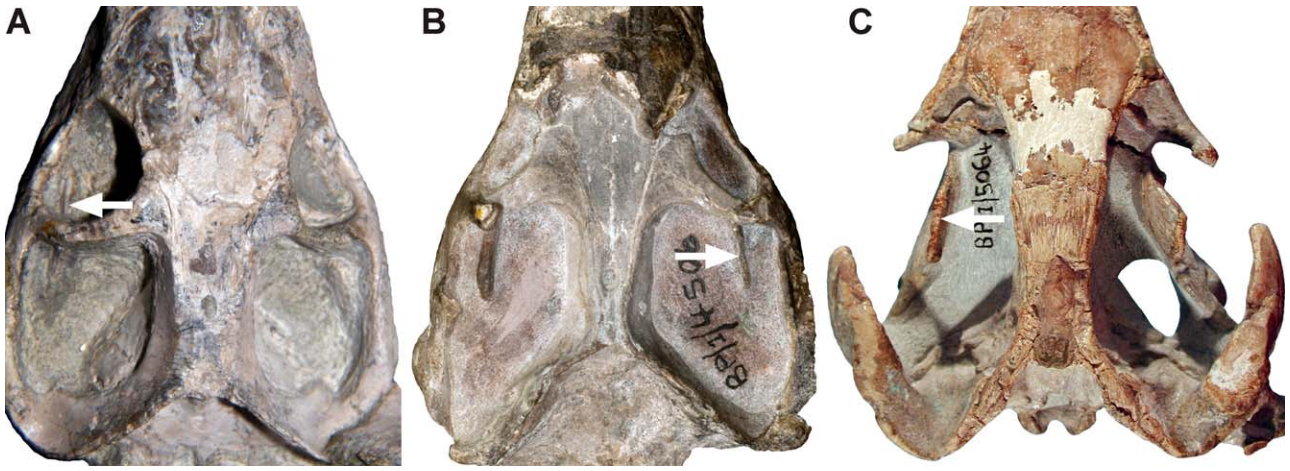

Fig. 13. Position of the mandible relative to the zygomatic arch in immature and adult individuals of *Galesaurus*. Skulls are in dorsal view. (A) SAM-PK-K10465 (juvenile, BSL 67 mm); (B) BP/1/4506 (subadult, BSL 85 mm); (C) BP/1/5064 (adult, BSL 103 mm). The coronoid process (arrow) is near the middle of the temporal fenestra in adult individuals.

Fig. 14. Oblique ventroposterior view of the palate of BP/1/4506 (subadult, BSL 85 mm). Arrow indicates the posterolateral margin of the transverse pterygoid process near its contact with the medial edge of the mandible.

Galesaurus, the dorsal adductor fossa is deeper and the dorsal tip of the coronoid process is inflected slightly laterally (Figs. 13C and 15D).

DISCUSSION

Cranial Allometry in *Galesaurus planiceps*

The positive allometry of skull width (SW; Table 3) indicates that during ontogeny the zygomatic arches in dorsal view became laterally flared, although the skull is much wider in half of the sampled adult specimens (Fig. 2C,D). The resulting increase in the width of the temporal fenestra would have accommodated large, well-developed adductor muscles. The DBW is negatively allometric, suggesting that the relative narrowing of the temporal skull roof also contributed to the expansion of the temporal fenestra. The combination of these trends for the increased accommodation of the adductor musculature is also recognized in living mammals (e.g., Abdala et al., 2001).

The strong positive allometry of TEL (Table 3) indicates this region greatly lengthened during growth (Figs. 2 and 7) and suggests that the area of attachment of the temporalis musculature greatly increased during growth. The strong positive allometry of the height of the zygomatic arch also indicates that the attachment region for the masseter muscles became well-developed with increasing age.

The orbital length (OL) is negatively allometric and follows the expected trend for tetrapods (see Emerson and Bramble, 1993). Interestingly, the orbital diameter (OD) in *Galesaurus* shows isometry (Table 3), which is unlike the general trend for tetrapods but is similar to the trend of orbital length found for the three marsupials *Dromiciops gliroides* (Giannini et al., 2004), *Caluromys philander* (Flores et al., 2010), and *Echymipera kalubu* (Flores et al., 2013). However, a common connection between the relatively faster growing orbits of these three marsupial taxa and their lifestyle (behaviour, food habits, and habitat) could not be found (also see Flores et al., 2013).

Comparative allometry in non-mammaliaform cynodonts. In comparison with *Thrinaxodon*, the most significant differences for *Galesaurus* are positive

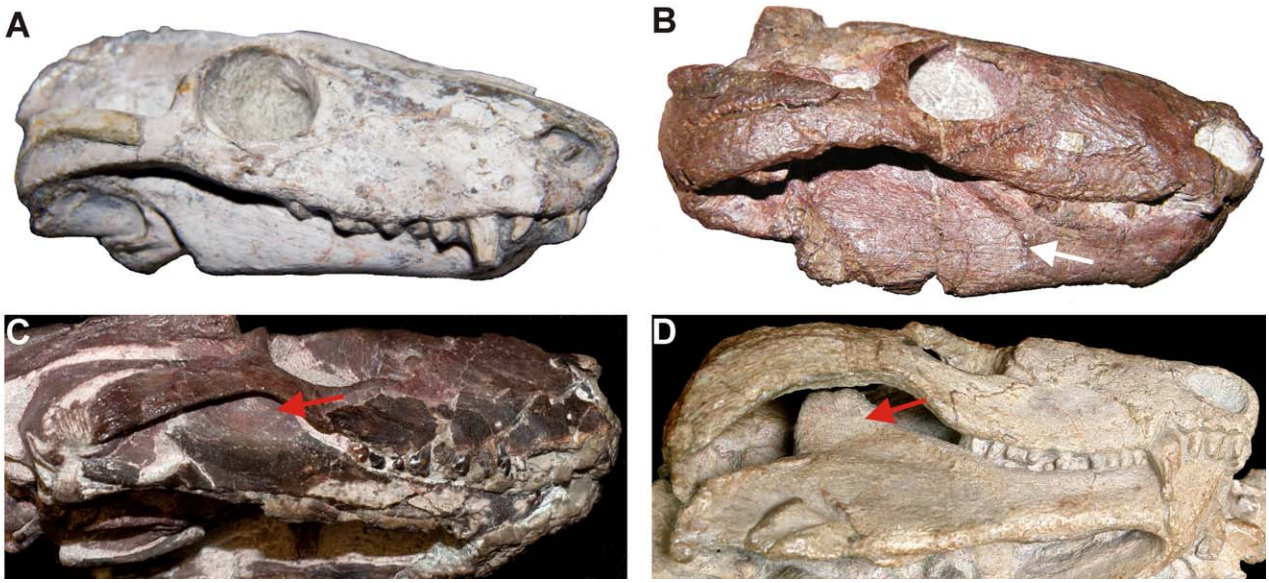

Fig. 15. The mandible of *Galesaurus* in lateral (A, B) and ventrolateral (C, D) views. (A) SAM-PK-K10465 (juvenile, BSL 67 mm; image is mirrored); (B) TM 83 (adult, BSL 94 mm) showing the presence of the anterior ridge of the masseteric fossa (white arrow); (C) NMP 581 (juvenile, BSL 64 mm); (D) NMQR 3542 (adult, BSL 102 mm). Red arrows in (C, D) point to the dorsal adductor fossa.

allometry for SW and ZH, negative allometry for BGW, and isometry for OD (Table 4). In addition, the MUL and PAL is isometric in *Galesaurus*, whereas they are positively allometric in *Thrinaxodon*. The scaling of the occipital plate height (OH) is also different between the two taxa (Table 4). The temporal region (TEL, POP, PSC, MTO) has strong positive allometry in both taxa, although the coefficients are much larger in *Galesaurus* (Table 4).

The positive allometry of ZH in *Galesaurus* suggests that the masseters became more developed with growth than in *Thrinaxodon*, and the SW indicates an enlargement of the temporal fenestra to accommodate these muscles. The difference of isometry in the PAL in *Galesaurus* and the positive allometry in *Thrinaxodon* might be related to the development of a longer secondary palate in the latter taxon. The positive allometry of OH in *Thrinaxodon* indicates a greater increase in the height of the posterior sagittal crest but also an increase in the height of the apex of the lambdoidal crest during ontogeny; whereas OH is isometric in *Galesaurus*.

The eucynodonts and *Galesaurus* both have positive allometry in the temporal region (TEL, SW, and ZH) (Table 4). The OH and OW (occipital plate width) are isometric in *Galesaurus*, *Massetognathus*, and *Chiniquodon* (Table 4).

There are some overall interesting trends observed in the sampled cynodonts (Table 4). The UP is isometric in basal cynodonts and *Chiniquodon*; whereas it is negatively allometric in the two gomphodonts *Diademodon* and *Massetognathus*. The maxillary bicanine width (BW) is isometric in all of the cynodont taxa except *Chiniquodon* that has a positive allometry. Considering orbital trends, the OL is isometric in *Chiniquodon* but negatively allometric in the other cynodonts (no data in *Diademodon*); whereas the OD is isometric in *Galesaurus* and negatively allometric in the remaining cynodonts (no data in *Chiniquodon*). The IO is isometric in all cynodonts (Table 4).

Qualitative Differences during Ontogeny

The changes in the craniomandibular apparatus that occurred during the ontogenetic development of *Galesaurus planiceps* are listed in Table 5.

Nasal-frontal suture. In all specimens of *Galesaurus*, the ectocranial morphology of the nasal-frontal suture is an inverted V-shape. In the adult specimen of *Progalesaurus*, the nasal-frontal suture is also inverted V-shaped (Sidor and Smith, 2004), although the frontal projection does not reach the anterior margin of the orbit.

In *Thrinaxodon*, however, the nasal-frontal suture morphology changed with ontogenetic age: juveniles have an inverted V-shaped suture, subadults have either an inverted V-shaped suture, transverse suture or an intermediate morphology, and most adults have a transverse suture (Jasinoski et al., 2015). However, in a few adult *Thrinaxodon* specimens, the suture is an inverted V-shape (Jasinoski et al., 2015), which suggests that the tendency to have this morphology at the adult stage was still present. The anterior frontal projection in the juveniles of *Thrinaxodon* is relatively shorter than in immature (non-adult) specimens of *Galesaurus*.

An ontogenetic survey of this suture is required for other basal cynodonts to determine if there is a phylogenetic trend (see Fig. 1).

Nasal-nasal suture. During the ontogeny of *Galesaurus*, the nasal–nasal suture on the surface of the snout changed from a relatively straight suture with few interdigitations to an interdigitated suture (Table 5).

TABLE 5. List of craniomandibular features of *Galesaurus planiceps* that changed during ontogeny

Character	BSL (mm)	Ontogenetic Stage	Cranial Region
Nasal-nasal suture: relatively straight on surface, 1-2 interdigitations near mid-length of snout	≤64	Juvenile	Snout
Nasal-nasal suture: numerous small interdigitations on the snout	≥69	Subadult, Adult	
Posterior projection of postorbital: ventral process longer than dorsal process	≤67	Juvenile	Temporal
Posterior projection of postorbital: dorsal and ventral processes are subequal in length	≥69	Subadult, Adult	
Sagittal crest is not developed	≤85	Non-adult	Temporal
Posterior sagittal crest is present	≥88[a]	Adult	
Angulation of the zygomatic arch is absent	≤88[b]	Non-adult	Zygoma
Angulation of the zygomatic arch is present	≥90[c]	Adult	
External occipital crest and parasagittal fossae are not prominent	n/a[d]	Younger	Occiput
External occipital crest and parasagittal fossae are more prominent and well-developed	n/a[d]	Older	
Sutures between exoccipital and the supraoccipital, opisthotic, basioccipital are patent	≤88	Non-adult	Occiput
Sutures between exoccipital and the supraoccipital, opisthotic, basioccipital are fused	≥90[e]	Adult	
Mandible positioned in close proximity to the zygomatic arch (lateral position)	≤85	Non-adult	Mandible
Mandible positioned near the middle of the temporal fenestra (middle position)	≥88	Adult	
Anterior ridge of the masseteric fossa is absent	≤88	Non-adult	Mandible
Anterior ridge of the masseteric fossa is present	≥90[f]	Adult	

From these qualitative characters, the present sample of *Galesaurus* can be divided into three ontogenetic stages: juvenile (BSL ≤ 67 mm), subadult (69–88 mm), and adult (BSL ≥ 90 mm). Non-adults include both the juvenile and subadult individuals.
[a]In specimens AMNH 2223 and NMQR 860, the condition of the sagittal crest is equivocal due to over-preparation and/or taphonomic processes.
[b]Specimen BP/1/4714 is an exception.
[c]Specimens BP/1/2513A and TM 83 are exceptions.
[d]A non-discrete character, so a numeric division between skull sizes is not possible.
[e]Specimens BP/1/4714 and SAM-PK-K8549 are possible exceptions.
[f]Specimen SAM-PK-K10468 is an exception.
Abbreviations: BSL, basal skull length; n/a, not applicable.

This differs from *Thrinaxodon*, in which the suture showed no clear ontogenetic pattern (Jasinoski et al., 2015). In *Thrinaxodon*, most specimens have a fairly straight suture with interdigitations mostly confined to the midlength of the snout (see Jasinoski et al., 2015: fig. 6A), which is similar to that observed in the small specimens of *Galesaurus* (Fig. 5A).

The difference in suture morphology might also indicate that the snout of *Galesaurus* is more rigid than in *Thrinaxodon*.

Secondary palate. The degree of openness of the secondary palate of *Galesaurus* is similar in all ontogenetic stages. Abdala (2007) stated that the palatine bones are relatively shorter in specimens NMQR 860 and BP/1/5064 compared with AMNH 2223, indicating variability of this feature. However, our observations of the secondary palate in the larger sample of *Galesaurus* indicate that in all specimens the palatines only contribute a small portion to the secondary palate.

In both *Galesaurus* and *Thrinaxodon*, the anterior part of the secondary palatal cleft is wider than the posterior part. However, in *Galesaurus* the palatal cleft is relatively wider and the length of the secondary palate is relatively shorter (Fig. 6) compared with *Thrinaxodon* (Jasinoski et al., 2015: fig. 7); the latter difference is due to the shorter maxillae in *Galesaurus*.

Interpterygoid vacuity. An interpterygoid vacuity is absent from all observed specimens of *Galesaurus* (Table 2). In contrast, a paired interpterygoid vacuity is present in early juveniles of *Thrinaxodon* but is absent from subadult and adult specimens (BSL ≥ 56 mm; Jasinoski et al., 2015). In the more basal epicynodont *Cynosaurus*, it is also present in a juvenile specimen and absent from the adult specimen (Van den Brandt, 2013). The interpterygoid vacuity is also absent from the adult specimen of *Progalesaurus* (Sidor and Smith, 2004). An interpterygoid vacuity, however, is present in the adult forms of the more primitive basal cynodonts *Procynosuchus* (e.g., Brink, 1963) and *Dvinia* (Tatarinov, 1968), as well as in the epicynodont *Platycraniellus* (Abdala, 2007).

Therefore, an interpterygoid vacuity appears to be a plesiomorphic character of basal epicynodonts, present in at least the early juvenile stage. Considering the condition represented in *Cynosaurus* (Fig. 1), it is possible the vacuity was present in specimens of *Galesaurus* that are smaller than those recorded to date (see Table 2). This feature remains equivocal for *Galesaurus* until smaller specimens are found.

Frontal-parietal suture. The ectocranial morphology of the frontal–parietal suture in *Galesaurus* cannot be comprehensively documented across all ontogenetic stages; therefore it is uncertain if it changed with increasing age or it was affected by individual variation. In *Thrinaxodon*, the late juvenile stage had a transverse morphology, whereas it was interdigitated (M-shaped morphology) in the early juvenile, subadult, and adult stages (Jasinoski et al., 2015: table 6). The adult specimen of *Progalesaurus* also has a M-shaped frontal-parietal suture near the midline of the skull roof (see Sidor and Smith, 2004: fig. 3).

Frontal parasagittal depressions. The paired frontal parasagittal depressions were found only in three specimens with a BSL $\geq$ 102 mm (Table 2; Fig. 2D), but more well-preserved specimens are needed to confirm that this is an ontogenetic feature of large adult individuals of *Galesaurus*. The function of these depressions is unknown, and they are unlikely related to muscle attachment.

Paired parasagittal depressions on the frontal bones have been previously described in the eucynodont *Chiniquodon* (Teixeira, 1982). These depressions are similar to *Galesaurus*, but in MCP PV1600 [type specimen of *Probelesodon kitchingi* = *Chiniquodon theotonicus*, after Abdala and Giannini (2002)] the depression covers nearly the entire frontal bone because the skull roof is narrower, and the frontal–frontal suture is raised as a sharp ridge (see Teixeira, 1982: pl. I). These depressions occur in mid to large chiniquodontid specimens (e.g., MCP PV1600; BSL 164 mm from Abdala and Giannini [2002: table 1]). In addition, frontal depressions developed in intermediate and large specimens of *Dadadon isaloi*, a traversodontid (Kammerer, et al., 2012).

Posterior projection of the postorbital. During the ontogeny of *Galesaurus*, the posterior projection of the postorbital changed in morphology. In juvenile specimens of *Galesaurus* (BSL $\leq$ 67 mm), the ventral process is much longer than the dorsal process; whereas the processes are subequal in length in subadult and adult individuals (BSL $\geq$ 69 mm). This change in morphology is similar to the pattern observed for *Thrinaxodon* that occurred during the transition from late juvenile to the subadult stage (Jasinoski et al., 2015). Therefore it appears that *Thrinaxodon* and *Galesaurus* developed subequal processes of the posterior projection of the postorbital at the same relative ontogenetic stage.

In most basal epicynodonts, the posterior projection of the postorbital is comprised of two processes that became longer during ontogeny. In *Cynosaurus*, the most basal epicynodont (Fig. 1), the ventral process developed before the dorsal process (e.g., juvenile specimen BP/1/4469) and the adult has two subequal processes (BP/1/3926). In the adult *Progalesaurus*, the projection is divided forming a forked morphology (Sidor and Smith, 2004). *Thrinaxodon* has two subequal processes in subadult and adult individuals, but in juvenile specimens (BSL $\leq$ 42 mm) the ventral process is much longer than the incipient dorsal process (Jasinoski et al., 2015), similar to what was observed in small specimens of *Cynosaurus* and *Galesaurus*. However, in the most derived basal epicynodont *Platycraniellus* (Fig. 1), only a single, undivided projection is present in the adult specimen (Abdala, 2007).

Sagittal crest development. In most specimens of *Galesaurus*, only the posterior sagittal crest became fully developed during ontogeny. The only unequivocal exception is specimen SAM-PK-K10468, which also developed a narrow anterior sagittal crest. This specimen is close to the maximum size for *Galesaurus* (Table 2; note that NMQR 860 has an eroded intertemporal region), and it presumably represents an old (senescent) individual. Therefore, it is possible that the anterior sagittal crest developed only in old individuals, or it may represent individual variation.

The adult specimen of *Progalesaurus* also lacked development of an anterior sagittal crest (Sidor and Smith, 2004).

In contrast to the galesaurids, the anterior sagittal crest is present in all adult specimens of *Thrinaxodon* (Jasinoski et al., 2015). The lack of development of the anterior sagittal crest in most *Galesaurus* specimens suggests that the anterior fibres of the temporalis musculature of *Galesaurus* were not as well-developed as in *Thrinaxodon*.

The posterior sagittal crest developed in *Galesaurus* specimens with BSL $\geq$ 88 mm, close to the transition to adulthood, which is relatively much later in ontogeny than in *Thrinaxodon* (BSL $\geq$ 42 mm, late juvenile stage; Jasinoski et al., 2015). This later development also indicates that the temporalis was proportionately smaller in the immature specimens of *Galesaurus* relative to similar-sized specimens of *Thrinaxodon*.

A heterochronic shift in the development of the sagittal crest has been proposed for some species and populations of *Lynx* (Garcia-Perea, 1996). A survey of the variation across four species of *Lynx* (and across different populations of a single species) showed that the sagittal crest is not fully developed (i.e., not extended along the total length of the parietal suture) in some adult species and it can differ between some populations (Garcia-Perea, 1996). In the species that only developed the posterior part of the sagittal crest, it was suggested that these species are paedomorphic in comparison to the hypothetical ancestral pattern (Garcia-Perea, 1996). Taking this into consideration, it appears that *Thrinaxodon*, which was more derived than *Galesaurus* (Fig. 1), showed accelerated development in relation to the posterior sagittal crest. In addition, the ontogenetic delay between the development of the posterior sagittal crest (late juvenile stage) and the anterior sagittal crest (adult stage) in *Thrinaxodon* (Jasinoski et al., 2015) suggests that the anterior crest in *Galesaurus* might not have manifested until much later in its ontogeny. Therefore, it is not surprising that the anterior sagittal crest only developed in the second largest specimen of *Galesaurus* (Table 2).

Parietal-parietal suture. The ontogenetic condition of the posterior parietal-parietal suture is variable for *Galesaurus*. In one of the smallest specimens of *Galesaurus* (FMNH PR 1774), the posterior parietal-parietal suture remained patent across the depth of the parietals. In some of the larger specimens (BSL $\geq$ 69 mm), there are deposits of new bone dorsal to the suture;

however, the suture was visible on the dorsal surface of the skull in four specimens with BSL ~71–81 mm. Therefore, it is assumed that the dorsal deposition of bone onto the posterior parietal-parietal suture began at 69 mm BSL if not earlier, and there is variation in the timing of this deposition. Because of the lack of well-preserved specimens and the absence of a clear pattern regarding the dorsal obliteration of the posterior parietal-parietal suture, at this time we cannot use this feature as an ontogenetic indicator.

In contrast, *Thrinaxodon* showed a clear pattern of progressive dorsal deposition of bone that increased in thickness with ontogenetic size (Jasinoski et al., 2015: fig. 12). In addition, the posterior parietal-parietal suture was not visible on the dorsal ectocranial surface in juvenile specimens of *Thrinaxodon* (Jasinoski et al., 2015) [but note a single exception: further preparation of two small *Thrinaxodon* skeletons (block SAM-PK-K8004b,c) revealed disarticulated cranial material (BSL 31–36 mm; pers. obs.) of which there is a dorsally-patent posterior parietal-parietal suture]. New bone was therefore already deposited dorsal to the suture at an early juvenile ontogenetic stage of *Thrinaxodon* even though the posterior sagittal crest was not yet developed (Jasinoski et al., 2015).

In the adult specimen of *Progalesaurus*, the posterior parietal-parietal suture is not visible on the dorsal surface of the skull roof (Sidor and Smith, 2004), which suggests that new bone was deposited on top of the suture.

The anterior parietal–parietal suture appears to be patent in all ontogenetic stages of *Galesaurus*, although its condition is equivocal in the large adult specimens. This pattern of patency across all ontogenetic stages was also observed in the comprehensive ontogenetic survey of *Thrinaxodon* (Jasinoski et al., 2015). The adult specimen of *Progalesaurus* also has a patent anterior parietal–parietal suture.

Angulation of the zygomatic arch. Angulation of the zygomatic arch is an ontogenetic feature of *Galesaurus* (Table 5). The presence of this feature in nearly all of the large specimens of *Galesaurus* (BSL $\geq$ 90 mm) suggests that the adults had a much more developed superficial masseter muscle than the immature individuals.

It was proposed that the superficial masseter was present at the epicynodont stage, but absent at the base of the cynodonts (Abdala and Damiani, 2004; Fig. 1). However, the only well-preserved adult skull of *Cynosaurus* (BP/1/3926) does not have angulation of the zygomatic arch; therefore it is possible that the superficial masseter was not divided in this basal epicynodont taxon. Angulation of the zygomatic arch is present in the adult epicynodont specimens of *Progalesaurus*, *Galesaurus*, and *Platycraniellus* (Abdala, 2007). Its absence from the majority of large adult *Thrinaxodon* specimens (Jasinoski et al., 2015) suggests that the superficial masseter was not as well-developed in these adults relative to the adult *Galesaurus*.

Flaring of the zygomatic arch. The zygomatic arches of *Galesaurus* became more laterally flared with age (SW; Table 3). However, in half of the sampled adult *Galesaurus* specimens, the zygomatic arches appear much more laterally flared, which suggests that the adductor muscles became much more developed in those individuals. This difference between adult specimens is further investigated in relation to sexual dimorphism (see section "Variation within *Galesaurus*," below).

Squamosal sulcus. It appears that the development of the squamosal sulcus is variable within *Galesaurus*, as only three adult specimens have a relatively deep sulcus.

The squamosal sulcus has been considered possibly for the passage of the external auditory meatus (see Allin, 1975: pl. 4, fig. 19; Allin and Hopson, 1992) or for the attachment of the depressor mandibulae (Allin 1975: pl. 6, fig. 26E). In *Galesaurus*, the dorsal shelf of bone that forms the squamosal sulcus continues anteriorly for a short distance along the posterolateral part of zygomatic arch. In some cynognathians, the structure in the zygoma developed into a robust sulcus [e.g. *Cynognathus* (BP/1/4664), *Trirachodon* (BP/1/4658), *Massetognathus* (PVL 5441, BP/1/4245)], and it is assumed that it was the site of origin for the depressor mandibulae (jaw opening muscle) because a similar dorsal position of this muscle occurs in chelonians (Werneburg, 2011) and lizards (Iordansky, 1970). Therefore, we consider the squamosal sulcus as being the origin of the depressor mandibulae.

Orbit orientation. During the ontogeny of *Galesaurus*, the orientation of the orbits changed from a lateral orientation in immature specimens (Fig. 10A) to a more anterior orientation in at least half of the sampled adult individuals (Fig. 10B). The change in orbit orientation in these adult specimens is partially due to the extensive flaring of the zygomatic arches (which includes the infraorbital arch).

A change in visual orientation during ontogeny has not been documented before in any other non-mammaliaform cynodont. In all ontogenetic stages of *Cynosaurus*, the orbits face mostly laterally (see Van den Brandt, 2013: fig. 8). A re-examination of the ontogenetic series of *Thrinaxodon* revealed that there is a change in orbit orientation, in which the orbits face more anterolaterally in larger individuals (see Jasinoski et al. [2015]: figs. 2 and 5). In the adult *Probainognathus*, the orbits have a distinctive anterodorsal orientation (Romer, 1970), but this orientation is also the same in a juvenile individual (PVL 4169; F. Abdala, pers. obs.).

Orbital convergence has been considered in several modern mammals (e.g., Cartmill, 1972; Noble et al., 2000; Heesy, 2004). Orbital convergence has a strong linear correlation with increasing binocular visual field overlap in mammals (Heesy, 2004). Therefore, mammals with highly convergent orbits have better binocular vision; whereas species with laterally-facing orbits have a wide panoramic visual field (Heesy, 2004). Eutherian taxa that are nocturnal or cathemeral tend to have more convergent orbits than diurnal taxa; carnivorous and omnivorous taxa have more convergent orbits than non-carnivorous or opportunistic taxa (Heesy, 2008). Highly convergent orbits do not necessarily indicate an arboreal lifestyle (e.g., Cartmill, 1972; Heesy, 2008).

Allometry of orbital convergence has rarely been investigated during the growth of a single modern

species. In a recent ontogenetic study of giraffes, it was discovered that the amount of binocular overlap increased with age, with adults having less panoramic vision than neonates (Mitchell et al., 2013). Comparisons across taxa have shown that orbital convergence and skull size are positively correlated in herpestids (Noble et al., 2000). Thus larger herpestid taxa have more convergent orbits than the smaller ones, but behavioural studies are required to determine if the former engage in more nocturnal activities that require highly convergent orbits (Noble et al., 2000).

A change in orbit orientation due to geographic isolation has been documented in a bovid species (Köhler and Moyà-Solà, 2004). The extinct island species *Myotragus* had a more anterior orbit orientation compared to its closest living relative that resides on the continent (Köhler and Moyà-Solà, 2004). This shift was attributed to lack of predation pressure on the island because an anterior orbit orientation is atypical of a prey species that normally depends on a large panoramic field of vision provided by a lateral orientation of the orbits (Köhler and Moyà-Solà, 2004). In addition, the orbit and brain size was smaller in comparison to its mainland relative (Köhler and Moyà-Solà, 2004).

It has been documented in some eutherian mammals that the relative size of the adductor muscles correlates with the position of the orbits (Cox, 2008). Mammals with a dominant temporalis muscle (e.g., Carnivora) have a more anterior orientation (increased orbital convergence), but those with a dominant masseter (e.g., rodents, lagomorphs) tend to have a lateral orientation of the orbits (Cox, 2008). However, these specific observations in eutherian mammals can only be tentatively applied to the basal cynodonts because the deep masseter had a posterodorsal orientation unlike the anterodorsal orientation in several mammals (see Turnbull, 1970). In *Galesaurus*, which has a well-developed postorbital bar, it is predicted that the masseters and not the temporalis muscle were instead the main influence on the orientation of the orbits, based on changes in the zygomatic arch associated with the development of these muscles.

Clearly habitat, lifestyle, and masticatory musculature can influence the orientation of the orbits. It is possible that the adductor musculature in *Galesaurus* was the main factor for the flaring of the zygomatic arches, and that the orbits became more anterior facing as a side-effect of the flared arches. The change in orientation of the orbits may also indicate that there was a shift during ontogeny to a more nocturnal lifestyle or more active predation.

External occipital crest. The external occipital crest occurs in all ontogenetic stages of *Galesaurus*, and it increased in prominence with an increase in skull size.

The structure of the external occipital crest in *Galesaurus* is similar to that of the closely-related *Progalesaurus*, but is unlike that of *Thrinaxodon*. In *Galesaurus*, the long crest occurs both on the interparietal and supraoccipital, and the lateral depressions became more prominent with age. In *Thrinaxodon*, the crest is generally poorly developed and it mainly formed on the interparietal (and only rarely on the supraoccipital) of large subadult and adult *Thrinaxodon* (BSL $\geq$ 61 mm; Jasinoski et al., 2015). It was assumed that this low crest that developed later in ontogeny indicated relatively weak nuchal muscles in *Thrinaxodon* (Jasinoski et al., 2015). In contrast, the ubiquitous and longer crest in *Galesaurus* might indicate that the nuchal muscles were much more developed.

Foramen magnum. In *Galesaurus*, the foramen magnum has either a circular shape or a dorsal notch, but this difference does not appear to coincide with the size of the individual. Interestingly, variation in shape of the foramen magnum has been observed in some smaller breeds of dogs, and the presence of a dorsal notch does not appear to affect function (Watson et al., 1989; Onar et al., 2013). The foramen magnum has a circular outline in *Thrinaxodon* and *Progalesaurus*, but it is distorted in the latter taxon.

The disparity in the presence and development of two projections along the dorsolateral edge of the foramen magnum also appears to reflect individual variation in *Galesaurus*.

Fusion of exoccipital with surrounding bones. In the adult specimens of *Galesaurus* (BSL $\geq$ 90 mm), the sutures between the exoccipital and the supraoccipital, opisthotic, and basioccipital became fused. This is a distinctive ontogenetic feature of *Galesaurus* that can be used to divide immature from adult individuals (with two possible exceptions; Table 5).

The fusion of these three sutures created a solid occipital plate surrounding the foramen magnum (Fig. 12C,D). Fusion of the four occipital bones would have stabilized the occiput and helped to protect the spinal cord and brain. The large external occipital crest of *Galesaurus* suggests that it had well-developed neck muscles, and a fused occipital plate would have protected the occiput from deformation during movements of the head and during locomotion.

In the adult specimen of *Progalesaurus*, there is no fusion of the exoccipital with the surrounding occipital elements (see Sidor and Smith, 2004: figs. 4 and 5). Perhaps fusion did not occur in this taxon, but additional large specimens of *Progalesaurus* are required to confirm this supposition.

Specimens of *Thrinaxodon*, including previous serial sectioned and micro-CT and CT scanned specimens, were re-investigated to determine if fusion similar to that observed in adult *Galesaurus* occurred during ontogeny. During our original survey (Jasinoski et al., 2015), the ventral half of the occiput in most large adult specimens was either not prepared (e.g., TM 166; NMQR 1416 [subsequently prepared but the occiput was badly crushed]) or poorly-preserved (e.g., NMQR 809, NMQR 1864). In a serial section of a large adult *Thrinaxodon* (BSL 88 mm; Broom, 1938: fig. 2, section 18) a suture is present between the exoccipital and basioccipital, and the exoccipital and the opisthotic. However, Broom's (1938: fig. 2) interpretive drawing and description of section 17, a more anterior section of the skull, suggested that the exoccipital and opisthotic might be partially fused to the right of the supraoccipital bone; however, his interpretation cannot be confirmed because he did not photograph the serial section and the left side of the

occiput does not show the same configuration (see Broom, 1938: fig. 2, section 17). On the contrary, smaller individuals of *Thrinaxodon* do not show any evidence of fusion of the occipital elements. This includes the serial-sectioned subadult (dorsal skull length of 67 mm; see Fourie, 1974: fig. 29) and the CT-scanned adult specimen UCMP 40466 (BSL 74 mm; see Rowe et al., 1995). In addition, the micro-CT scan of the adult BP/1/7199 (BSL 75 mm) shows a clear sutural gap between all of the occipital elements, and the gross morphology and micro-CT sections of TM 180 (BSL 75 mm) indicate that the occipital sutures are patent. Unfortunately, the largest micro-CT scanned *Thrinaxodon* specimen BP/1/5905 (BSL 87 mm) has poor resolution and the condition of these sutures could not be determined. Taking into account the available evidence, we postulate that fusion of the occiput did not occur in adult specimens of *Thrinaxodon*.

Fusion of the occipital elements has been documented in the derived probainognathian eucynodonts. In *Probainognathus*, the occipital bones are fused, with only the tabulars and interparietal having distinct sutures (Romer, 1970). This is a similar pattern to *Chiniquodon*, as observed in an intermediate-sized specimen (PVL 4444; Abdala, 1996). In the subadult specimen of *Lumkuia*, the suture between the exoccipital and the supraoccipital is indistinct (Hopson and Kitching, 2001), which may indicate that these elements are fused. In the mammaliaform *Morganucodon*, the exoccipital–basioccipital is fused, but the exoccipital-supraoccipital remained patent (Kermack et al., 1981). However, the exoccipital-supraoccipital is fused in the tritylodont *Oligokyphus* (Kühne, 1956). Therefore, there are some differences in the pattern of occipital fusion in these derived eucynodonts.

In modern mammals, fusion of the exoccipitals with surrounding bones (basioccipital, supraoccipital) is one of the earliest fusion events, occurring soon after or near the same time as the obliteration of the parietal-parietal suture (e.g., Sánchez-Villagra, 2010; Rager et al., 2014: fig. 1). Note that in modern mammals the opisthotic bone is part of the petrosal (Kielan-Jaworowska et al., 2004).

Position of the mandible in the temporal fenestra. A phylogenetic character describing the relative position of the mandible within the temporal fenestra (lateral or middle) has been used several times in cladistic analyses of derived therapsids (e.g., Hopson and Barghusen, 1986: char. 11.2; Sidor and Smith, 2004: char. 33; Abdala, 2007: char. 51). In these studies, this character was coded as "middle" for *Galesaurus* and all other cynodonts. This coding is in agreement with our survey of the large specimens of *Galesaurus* (Table 5; Fig. 2B–D); however, these studies did not take into account the immature specimens of *Galesaurus* that have a "lateral" position of the mandible (Table 5; Figs. 2A and 13A,B). This lateral position present in immature *Galesaurus* specimens is the only occurrence documented so far in any non-mammaliaform cynodont. Immature specimens of *Galesaurus* share a similar, but not as extreme, condition as in therocephalians (see Barghusen, 1968: fig. 6); however, unlike *Galesaurus*, the mandible remained in a lateral position in the adult therocephalians even if the temporal fenestra became laterally expanded (e.g., *Theriognathus*; F. Abdala, unpublished data).

The laterally-positioned mandible in the immature specimens of *Galesaurus* would have left only a small space for the insertion of the masseter muscles onto the lateral side of the mandible (Figs. 2A, 13A,B, 14, and 15C). In therocephalians it was hypothesized that the deep masseter inserted onto the surangular (Crompton, 1963; Barghusen, 1968). However, in basal cynodonts the masseter inserted onto the lateral edge of the dentary (e.g., Crompton, 1963), therefore it is unlikely that small specimens of *Galesaurus* had a different insertion to that of other cynodonts. Instead, we hypothesize that the masseter muscles were poorly developed in the immature specimens of *Galesaurus* based on the structure of the zygomatic arch (absence of angulation of the zygomatic arch and non-flaring arches) and the absence of the anterior ridge of the masseteric fossa on the dentary.

The relative width of the transverse processes of the pterygoid (TP; Fig. 3B) imposed a constraint on the relative position of the mandible (Fig. 14). The ratio between TP and skull width (SW) is larger in immature specimens of *Galesaurus* than in adults. This indicates that the width of the transverse processes is proportionally narrower in adults relative to skull width. It is apparent that changes in both the transverse processes of the pterygoid and the masseter muscles resulted in the mandible being positioned more medially within the temporal fenestra of adults.

Adductor fossae. The development of an anterior ridge of the masseteric fossa is characteristic of adult *Galesaurus* (Table 5), which indicates that the deep masseter was well-developed in mature individuals.

The dorsal adductor fossa, which is the insertion point for the lateral part of the temporalis, is deeper in large specimens of *Galesaurus*, indicating that the temporalis also became more developed with age.

Summary of the Qualitative Ontogenetic Features

There are eight ontogenetic differences in the skull and mandible that were observed in the sample of *Galesaurus* (Table 5). These include changes related to suture morphology, structures that support the adductor musculature, and the occiput.

From these qualitative changes, the present sample of *Galesaurus* can be divided into three ontogenetic stages: juvenile (BSL $\leq$ 67 mm); subadult (69–88 mm); and adult (BSL $\geq$ 90 mm) stages (Table 5). It is interesting to note that the division between the gracile and robust postcranial morphs of *Galesaurus* (Butler, 2009: table 3) coincides with our division between subadult and adult *Galesaurus* that is based on craniomandibular differences (Table 5). This suggests that the division between the two postcranial morphs of *Galesaurus* is due to ontogenetic differences rather than sexual dimorphism. In addition, our designation of the subadult stage (BSL 69–88 mm) agrees with Butler's (2009) histological results of the long bones of specimens RC 845 (BSL 69 mm) and NMQR 3716 (BSL 75 mm), both which have multiple layers of circumferential endosteal lamellar bone

surrounding the medullary cavity suggesting they represent a non-juvenile stage.

Only two cranial ontogenetic features separate the juveniles from the non-juvenile (subadult and adult) stages (Table 5). However, the transition from subadult to the adult stage in *Galesaurus* is demarcated by five craniomandibular ontogenetic changes (Table 5).

There are two *Galesaurus* specimens that have a combination of subadult and adult features. With a BSL of 88 mm, specimen BP/1/4602 is near the transition between the subadult and adult stages. It has a patent occiput, a relatively short temporal region, and absence of both the angulation of the zygomatic arch (Fig. 2B) and the anterior ridge of the masseteric fossa, which are features of most subadults; however, its mandible is positioned near the middle of the temporal fenestra and the posterior sagittal crest is developed, which are both adult features. Specimen BP/1/4714 also appears to have developed two features that are characteristic of adults: angulation of the zygomatic arch and the possible fusion of the exoccipital-supraoccipital suture. However, this specimen has a BSL of only 81 mm (Table 2); therefore it clearly falls within the subadult category.

Ontogenetic Comparison of the Cranial Function of *Galesaurus*

Several craniomandibular features changed during the growth of *Galesaurus* (Table 5; Fig. 2), indicating that cranial function might have varied between the ontogenetic stages. Juveniles were characterized by a relatively short dorsal process of the postorbital projection, which became subequal in length to the ventral process during the transition to the subadult stage. The extension of this projection increased the amount of bony overlap on the edge of the skull roof and may have increased stability of the postorbital bar that partially supported the anterior fibres of the temporalis muscle (see similar explanation for *Thrinaxodon* in Jasinoski et al. [2015] but note that the attachment of the anterior part of the postorbital bar to the skull roof was not as loose in *Galesaurus* as it was in *Thrinaxodon*). In addition, the increased number of ectocranial interdigitations in the nasal–nasal suture in subadult and adult *Galesaurus* (Fig. 5B,C) might indicate an increase in strain across the snout because the snout became more rigid.

Most of the changes in the skull occurred during the transition between the subadult and adult stages (Table 5). The angulation of the zygomatic arch developed in adults (Fig. 2C,D), indicating that the superficial masseter greatly increased in size, and the height of the zygomatic arch increased (Table 3), which suggests that the deep masseter was also well developed in adult *Galesaurus*. The medial shift of the mandible in adults (and the large subadult BP/1/4602) increased the space between the lateral edge of the mandible and the medial edge of the zygomatic arch for the insertion of the developing masseters (Fig. 2B–D), and the site of insertion onto the dentary became more apparent (Fig. 15B). The posterior sagittal crest developed (Fig. 7B–E) and the intertemporal region greatly lengthened (Table 3), creating a larger attachment area for the temporalis and indicating that this muscle became more developed in the adults. All of these changes suggest that the adult functioned differently than the immature individual (i.e., masseter and temporalis muscles were much larger). In addition, the external occipital crest became more prominent with increasing skull size, which indicates that the nuchal muscles became more developed with age. Fusion that occurred between four occipital bones at the adult stage (Fig. 12C,D) would have helped stabilize the occiput.

Variation within *Galesaurus*

There are a few cranial features that appear to exhibit intraspecific variability other than ontogenetic variation. This includes the morphology of the foramen magnum and the surrounding paired dorsolateral projections, which varied across all ontogenetic stages. The posterior parietal-parietal suture might have had an ontogenetic trend, but the inclusion of more well-preserved specimens is necessary to determine if all larger specimens have a dorsally obliterated suture or if this feature shows individual variation. The flaring of the zygomatic arches, changing of the orientation of the orbits, and deepening of the squamosal sulcus showed variation in the adult specimens. Because variation of the two former features divided the adult sample into two equal groups, the possibility of sexual dimorphism in *Galesaurus* was investigated.

Sexual dimorphism. Adult specimens of *Galesaurus* that were previously assigned to the taxon "*Glochinodontoides gracilis*" (synonymized with *Galesaurus* by Hopson and Kitching [1972]) have a wide skull with laterally flared zygomatic arches (see Haughton, 1924: fig. 50; Boonstra, 1935: fig. 1; Brink, 1954b: fig. 4; Table 1). On the contrary, *Galesaurus planiceps* (Owen, 1876: pl. XVIII, fig. 8) and "*Notictosaurus trigonocephalus*" (Brink and Kitching, 1951: fig. 8; Table 1) have a narrower skull. The holotype of the latter species is closely associated with two juveniles on block BP/1/2513, and has been interpreted as an adult female associated with its young (Brink, 1965). Therefore, it is hypothesized that adult specimens with a narrow skull might represent a "female" morph; whereas the wide skull morphology of "*Glochinodontoides*" might indicate a "male" morph.

We then reclassified the adult specimens as either "male" or "female" based on the skull width (Tables 1, 6) and replotted the allometric results from Table 3. The graph comparing the maximum skull width (indicative of flaring of the zygomatic arches) to BSL (Fig. 16A) shows that the "male" individuals plot above or on the regression line, confirming that their zygomatic arches are much wider than the "female" individuals that consistently plot below the slope. A *t*-test comparing measurements of SW between "males" and "females" was statistically significant (Table 7). It is interesting to note that the subadult individuals plot below the regression line, suggesting that the sexual dimorphism started at the adult stage (Fig. 16A). When the 'males' were excluded from the allometric analysis, the "females" still had positive allometry for SW ($b = 1.19$), but the value is not as strongly positive as when the "males" are also included in the analysis ($b = 1.56$; Table 3). This indicates that the zygomatic arches became laterally flared in all adult specimens, but the skull width increased to a greater extent in the "males."

The bivariate graph comparing the temporal region length with BSL shows that most of the "male" morphs have a longer temporal region that the "female" morphs (Fig. 16B), but this difference is not statistically significant under a *t*-test. The plot of the maxillary bicanine width (indicative of snout width) shows that most of the "male" morphs plot above the regression line (Fig. 16C); the difference between "males" and "females" is significant under a *t*-test (Table 7). The plots of snout length (Fig. 16D) and maximum zygomatic arch height show no clear separation between the morphs.

We also compared the variables relative to BSL to eliminate differences due to absolute size (see Simpson et al., 2003). The resulting ratios for the "male" and "female" morphs were compared in PAST using a *t*-test. The difference was significant for SW and marginally significant for TEL (Table 7). The latter result indicates that TEL is relatively longer in "males" only when this variable is scaled to BSL.

Principal component analysis of the complete data set discriminated between the three ontogenetic stages recognized by qualitative features through the PC1 (influenced by size), and split the adults into two groups based on shape alone (PC2) (Fig. 17A). Variables having high loads for PC2 are related to the temporal region (SW, TEL, MTO) and also include the width of the occipital plate (OW) and snout (BW). The "male" specimens are positioned in the upper right quadrant, indicating they have a wider skull (i.e., expanded temporal opening), longer temporal region and temporal opening, a wider occipital plate and snout; whereas a longer snout and skull characterize "female" specimens (Table 8; Fig. 17A). In summary, differences in shape of the snout, temporal region, and occipital plate are pronounced between "male" and "female" individuals.

The analysis with the reduced data set using GM scaling also shows a strong influence of variables describing the temporal region in the discrimination of groups (Fig. 17B). Here, the PC1 separated juveniles and subadults from adults with major contributions of BSL and MUL that positioned subadults and juveniles to the right of the first component and TEL influencing the position of adults to the left of the component (Fig. 17B; Table 8). The PC2 positioned adult "males" in the upper left quadrant by the influence of SW, and the only adult "female" of this reduced sample, which is located in the lower left quadrant, was influenced by MTO and ZH.

In the complete data set analysis, variables MUL and BSL separated adult "females" from "males" (Fig. 17A), but when size is eliminated, these variables separate adults from juveniles and subadults (Fig. 17B). The variable MTO has opposite loadings in the two analyses (Table 8). In the complete analysis MTO influences the position of adult "males"; whereas in the reduced data set analysis it strongly influences the placement of the only "female". This variation in MTO is the result of the reduction of data in the second analysis. In both analyses, SW has a strong influence in the discrimination of "males" (Fig. 17). Overall size change, accompanied by shape changes in the temporal region and occiput, differentiated between the adult sexual dimorphs of *Galesaurus*.

A relatively undeformed skull of a "male" morph (AMNH 2223; Fig. 18A) and "female" morph (NMQR 135; the dislocated squamosal and postorbital were taken into account; Fig. 18B) were scaled to the same basal skull length. The area of the temporal fenestra, a rough approximation of the size of the adductor muscles, was traced in both skulls (Fig. 18). The area of the temporal fenestra was much larger in the "male" morph, indicating that it had a larger development of the adductor musculature relative to the "female" morph.

TABLE 6. Adult specimens of *Galesaurus planiceps* re-classified as either a "male" or "female" morph

Specimen	BSL (mm)	Sexual dimorph
BP/1/3892[a]	90[a]	Female
BP/1/2513A[b]	90	Female[b]
NMQR 1451	90	Male
NHMUK 36220	92	Female
NMQR 135	94	Female
TM 83	94	Male
AMNH 2223	100	Male
NMQR 3340	~102	Female
NMQR 3542	102	Female
BP/1/5064	103	Male
SAM-PK-K10468	105	Male
NMQR 860	114	Male

See text for description of the sexual dimorphs.
[a]Specimen missing from collections; observations taken from Brink (1965).
[b]Specimen was interpreted as a 'female' based on its association with two juvenile individuals (Brink, 1965).
Abbreviation: BSL, basal skull length.

In some modern amphibians and reptiles, differences in head size and shape occur between the sexes. In many cases, the male has a larger head than the female resulting in a stronger bite, which could be either related to dietary divergence or sexual selection (e.g., Shine, 1989: appendix; Herrel et al., 1996; Vincent and Herrel, 2006). An ontogenetic study of the frogs *Rana ingeri* and *R. ibanorum* showed that males have wider and longer skulls than females, and were able to eat crabs at an earlier age than females presumably due to their more developed jaw musculature (Emerson and Bramble, 1993). However, it has been suggested for lizards that the larger head size in males (and hence, larger bite force) may have resulted from sexual selection (male-to-male combat) and that dietary divergence might be a secondary consequence, although more functional studies are required (Vincent and Herrel, 2006).

Taking these extant analogues into account, it is hypothesized that "males" of *Galesaurus* had a stronger bite force than "females" due to the larger attachment area for the adductor muscles. However, it is not possible to determine if this difference reflects a dietary difference between the sexes or antagonistic behaviour in the "males" of *Galesaurus*.

The wide, laterally flared zygomatic arches of the "male" *Galesaurus* appears to have indirectly influenced the orientation of the orbits: the "male" morph had a more anterior orientation of the orbits than the "female" morph (Fig. 18; Table 7). This difference in orbit orientation might have slightly increased binocular vision in the "males." Despite the difference in orbit orientation between the two morphs, the allometric plots of orbital diameter and length compared to BSL indicate that there is no sexually dimorphic difference regarding the size of the orbits (Table 7).

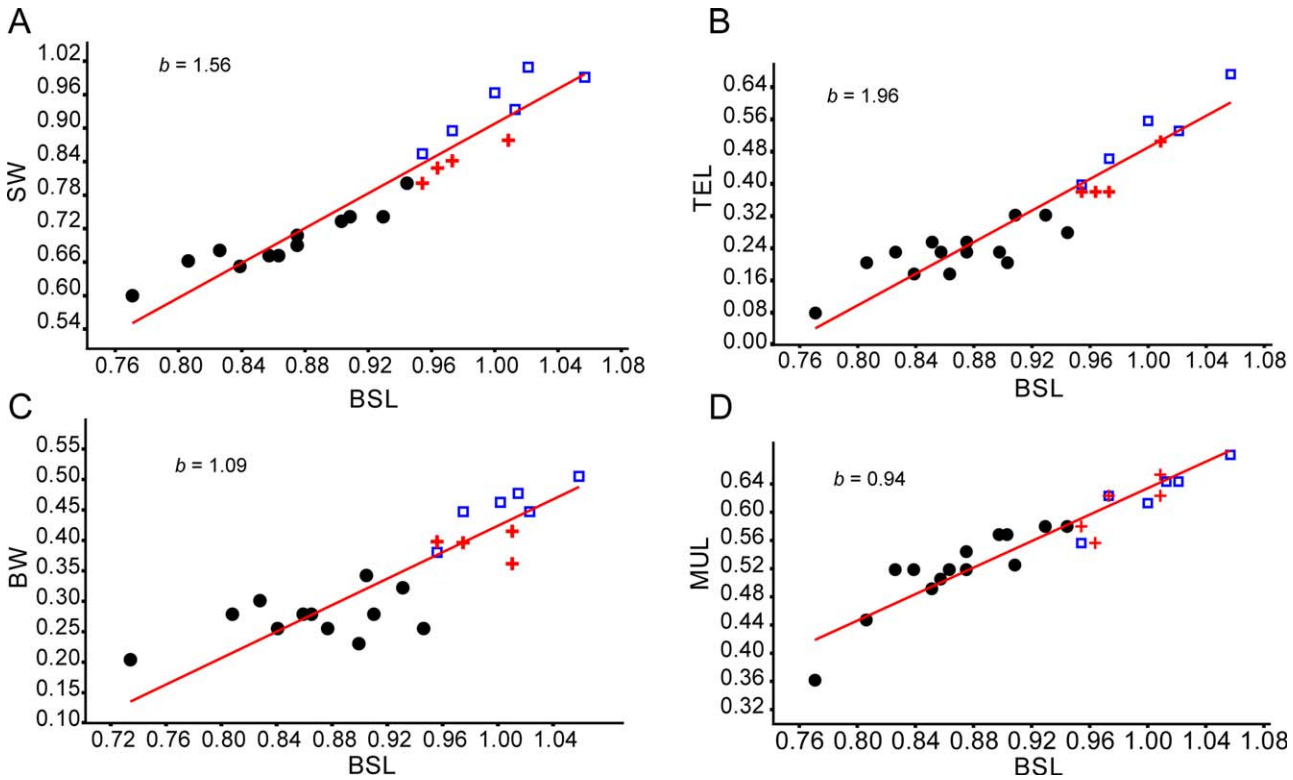

Fig. 16. Bivariate graphs after the adult specimens of *Galesaurus* were re-classified as either "male" (blue square) or "female" (red cross) based on skull width and previous taxonomic identification (see Tables 1, 6). Immature (non-adult) individuals are represented by black circles. (**A**) SW versus BSL; (**B**) TEL versus BSL; (**C**) BW versus BSL; (**D**) MUL versus BSL. Abbreviations: BSL, basal skull length; BW, maxillary bicanine width; MUL, muzzle length; SW, maximum skull width; TEL, temporal region length.

The morphology of the sagittal crest is a sexual dimorphic trait in some modern mammals. For example, the sagittal crest tends to be absent or poorly developed in female gorillas but it is usually more developed in the males, reflecting the larger area of attachment for the temporalis in males (Ashton and Zuckerman, 1956).

In our sample of *Galesaurus* there is only one unequivocal occurrence of an anterior sagittal crest; however, the sagittal crest region is eroded or damaged in a few large adult specimens. Therefore, at this time we cannot state if the anterior sagittal crest is due to sexual dimorphism or individual variation until further collection of well-preserved adult specimens. But it is interesting to note that the only occurrence of the anterior crest is in a large "male" morph (Table 6; Fig. 7D).

The depth of the squamosal sulcus might be a sexual dimorphic trait in *Galesaurus*, with the "male" morph having a deeper depression than the "female" morph (Table 7). However, more large adult specimens that have this area preserved are needed to confirm unequivocally this supposition. If it transpires that this feature is sexually dimorphic, we then hypothesize that the

TABLE 7. Cranial characters investigated for sexual dimorphism in *Galesaurus*

Character	Sexual dimorphic	"Male" condition	"Female" condition
Skull width (SW): lateral flaring of the zygomatic arch	Yes[a]	Wider	Narrower
Maxillary bicanine width (BW): width of snout	Yes[a]	Wider	Narrower
Length of snout (MUL)	No		
Temporal region length (TEL)[b]	Yes[c]	Longer	Shorter
Maximum height of zygomatic arch (ZH)	No		
Orbit orientation	Yes	More anterior	More lateral
Orbital diameter (OD)	No		
Orbital length (OL)	No		
Squamosal sulcus development	Equivocal[d]	Deep	Shallow

See Figure 3 for location of variables.
[a]Statistically significant under a *t*-test.
[b]Calculated using ratio TEL:BSL. See text for more details.
[c]Marginally significant ($P = 0.06$) under a *t*-test.
[d]More well-preserved specimens are required to determine if this is a sexual dimorphic feature.

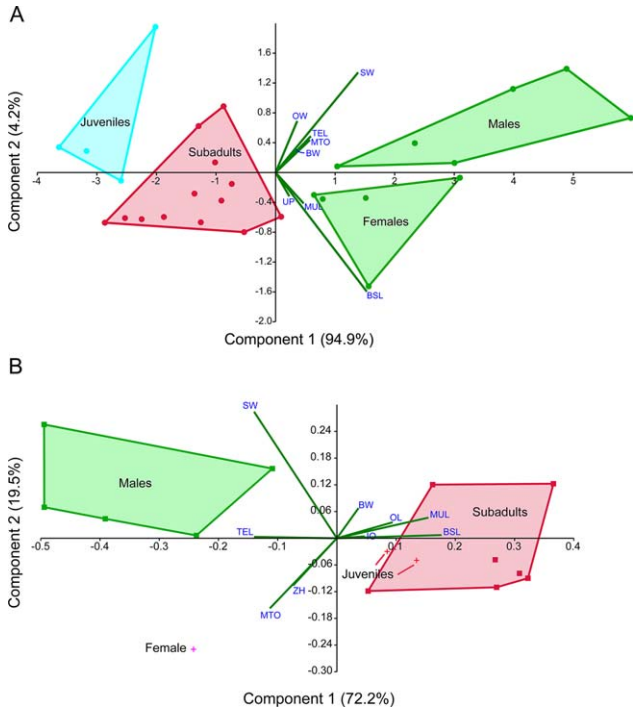

Fig. 17. Principal component analysis of cranial measurements of *Galesaurus*. (**A**) Complete data set includes 20 variables (Table 8) and 28 specimens (Table 2). (**B**) Reduced data set includes nine variables (Table 8) and 15 individuals; geometric mean was calculated for each individual and the raw data was scaled to the geometric mean to eliminate the influence of size. Green lines are the loading of the variables for the two components. Only the variables with the largest loads are represented in (A). The extreme location of the juvenile specimen BP/1/2513C in the upper left quadrant in (A) is the result of missing entries for all the variables with high loads for PC2. Abbreviations: PC1, principal component 1; PC2, principal component 2. See Figure 3 caption for abbreviations of variables.

TABLE 8. Results of the multivariate analysis of *Galesaurus planiceps*

	Complete data set		Size adjusted PCA	
Variable	PC 1	PC 2	PC 1	PC 2
BSL	0.6290	−0.6557	0.5000	0.0204
MUL	0.1935	−0.1704	0.4376	0.1311
NL	0.1063	−0.1023		
PAL	0.0451	0.0723		
BW	0.1448	0.1298	0.1034	0.1914
UP	0.0948	−0.1309		
OL	0.0417	0.0025	0.2666	0.1014
OD	0.0592	−0.0474		
IO	0.1158	−0.1073	0.1329	0.0118
TEL	0.2430	0.1999	−0.3956	0.0087
POP	0.0865	−0.0341		
PSC	0.0632	0.0432		
MTO	0.2370	0.1796	−0.3202	−0.4458
SW	0.5693	0.5512	−0.3955	0.8041
ZH	0.1452	0.0785	−0.2090	−0.3001
BB	0.0289	0.1000		
BGW	0.0162	−0.0227		
OH	0.0924	0.0196		
OW	0.1492	0.2839		
DBW	0.0334	−0.0304		

Loadings of the first two principal components are shown for two data sets: the complete raw data set, and the reduced data set that was size adjusted by using the geometric mean.
Abbreviation: PCA, principal component analysis. See Figure 3 for abbreviations of variables.

"males" would have had a larger jaw opening muscle than the "females."

Sexual dimorphism has been documented in only one other non-mammaliaform cynodont, *Diademodon* (Grine et al., 1978). The division between the two morphs of this eucynodont, however, could not be quantified, but was instead based on four qualitative cranial differences: (1) height and shape of the snout; (2) shape and orientation (lateral versus anterior) of the orbits; (3) development of the pterygoids; and (4) development of the "pterygosphenoid fossa" on the basioccipital (Grine et al., 1978). However, according to their figures (Grine et al., 1978: figs. 3 and 4), the orientation of the orbits appears to be anterolateral in both morphs, and differences are mainly reflected in the overall shape of the orbit with the "male" having a rounded orbit versus an ellipsoid orbit in the "female". The structure of the zygomatic arches was also mentioned as a possible difference separating the morphs, but its variability rendered it less diagnostic (Grine et al., 1978).

Grine et al. (1978) postulated that the four features separating the two morphs of *Diademodon* were neither sexually selective nor were they related to functional differences. This is in contrast to our hypothesis for *Galesaurus* (Table 7), in which differences in morphology between the two morphs, such as the lateral flaring of the zygomatic arches and the relative lengthening of the temporal region, may indicate a difference in cranial function.

Cranial Ontogeny of *Galesaurus* Compared to *Thrinaxodon*

A comparison of the cranial ontogeny of *Galesaurus* and the more derived basal cynodont *Thrinaxodon* (Jasinoski et al., 2015) revealed several differences, which include:

1. Zygomatic arch height has positive allometry in *Galesaurus* (ZH is isometric in *Thrinaxodon*; Table 4), which indicates that the masseter muscles, especially the deep masseter, were much more developed in older individuals of *Galesaurus* than in *Thrinaxodon*. A robust zygomatic arch would have been able to support a large attachment of the masseter, even if it just attached along the ventral edge of the zygomatic arch.
2. The development of the angulation of the zygomatic arch in the adult *Galesaurus* also suggests that the superficial masseter muscle became more developed relative to *Thrinaxodon*, which only rarely developed this feature.
3. The relative timing of the development of the posterior sagittal crest differs between the basal cynodonts. It appeared during the adult stage of *Galesaurus* (Table 5), whereas it developed at the late juvenile stage of *Thrinaxodon* (Jasinoski et al., 2015).

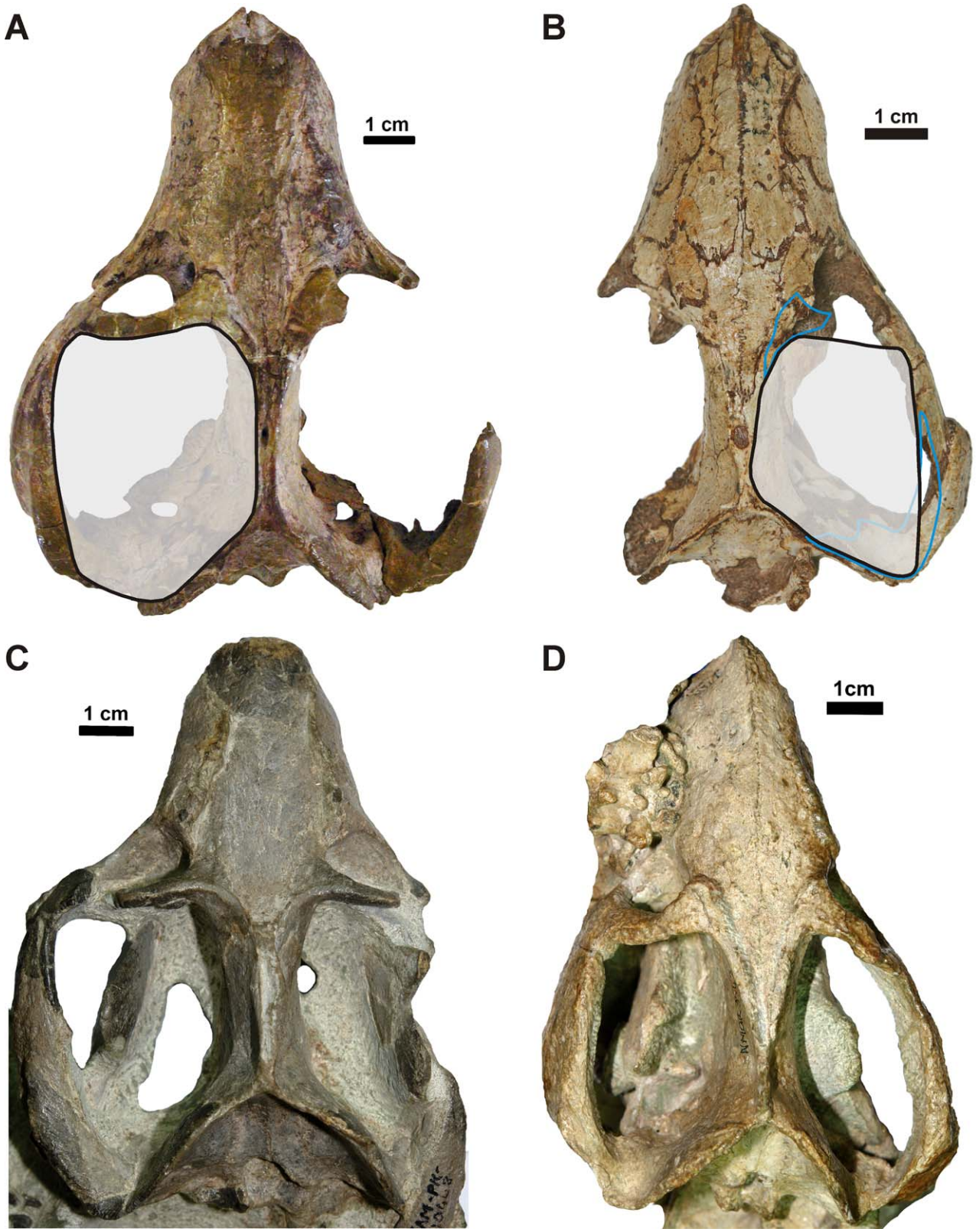

Fig. 18. Dorsal view of the skull of adult specimens of *Galesaurus* showing sexual dimorphism. (**A**) "Male" morph (AMNH 2223). (**B**) "Female" morph (NMQR 135; the disarticulated right postorbital and squamosal have been repositioned [blue outline]). (**C**) "Male" morph (SAM-PK-K10468). (**D**) "Female" morph (NMQR 3542). The skulls of AMNH 2223 and NMQR 135 were scaled to the same BSL, and the approximate area of the temporal fenestra, which estimates the size of the adductor muscles, is outlined. Note the area of the temporal fenestra is much larger in the "male" morph. Scale bars are 1 cm.

Therefore, the posterior sagittal crest had a relatively later development in *Galesaurus* compared to *Thrinaxodon*.

4. The anterior sagittal crest developed in all adult individuals of *Thrinaxodon*; whereas this structure was absent from the majority of *Galesaurus* specimens. This difference suggests that the anterior fibres of the temporalis muscle were less developed in *Galesaurus*.
5. Skull width, a measure of the lateral expansion of the zygomatic arches, is positively allometric in *Galesaurus*, but is isometric in *Thrinaxodon* (Table 4). This suggests that the adductor musculature was more developed in *Galesaurus*. Taking into account the previous four differences related to the adductor musculature in both taxa, and the large medial shift of the mandible within the temporal fenestra of *Galesaurus* (Table 5), it is hypothesized that the lateral expansion of the temporal fenestra reflects the greater development of the masseters in *Galesaurus*.
6. The external occipital crest of *Galesaurus* increased during growth, indicating an increase in the size of the nuchal muscles. In *Thrinaxodon*, an external occipital crest was absent in immature specimens and poorly developed in large subadults and adults (Jasinoski et al., 2015), suggesting relatively weaker nuchal muscles in *Thrinaxodon*.
7. *Galesaurus* attained a larger maximum skull size (BSL 114 mm; Table 2) than *Thrinaxodon* (BSL 96 mm; Jasinoski et al., 2015). However, both taxa appear to have indeterminate growth because of the presence of an unossified zone in the basicranium.
8. *Galesaurus* and *Thrinaxodon* reached the adult stage at different skull sizes. *Thrinaxodon* reached the adult stage at BSL 69 mm (72% of maximum adult size; see Jasinoski et al., 2015); whereas *Galesaurus* reached it at BSL 90 mm (79% of maximum adult size; Table 2). This might indicate that sexual maturity was reached relatively later in *Galesaurus*.

Only three features of the skull that changed during ontogeny were shared by *Galesaurus* and *Thrinaxodon*: (1) posterior projection of the postorbital; (2) posterior sagittal crest; and (3) external occipital crest (Table 5; Jasinoski et al., 2015). However, the ontogenetic timing and the degree of development of the two latter features differed between these basal cynodonts. The development of subequal processes of the posterior postorbital projection occurred during the transition to the subadult stage in both taxa.

There are four ontogenetic changes that only occurred in *Galesaurus* but not in *Thrinaxodon*: (1) large shift in the relative position of the mandible within the temporal fenestra; (2) change in ectocranial morphology of the nasal–nasal suture; (3) fusion of the exoccipital with three surrounding occipital bones (although further investigation of large, well-preserved adult *Thrinaxodon* specimens is required); and (4) development of sexual dimorphism at the adult stage.

There are a few characters in *Thrinaxodon* that changed during ontogeny, but are equivocal in *Galesaurus*: (1) presence of an interpterygoid vacuity in small juveniles (*Galesaurus* specimens smaller than BSL 54 mm are required); (2) change in the ectocranial trace of the frontal–parietal suture; (3) change in the shape of the parietal foramen; and (4) obliteration of the posterior parietal-parietal suture. Although there was no clear ontogenetic pattern for the obliteration of the posterior parietal–parietal suture in *Galesaurus*, the earliest unequivocal occurrence of dorsal obliteration was at BSL 69 mm (subadult stage). This is relatively late in ontogeny compared to *Thrinaxodon*, in which obliteration was apparent during the earliest ontogenetic stage (early juvenile; Jasinoski et al., 2015).

According to Butler's (2009) postcranial histological comparison of two similar-sized specimens of *Galesaurus* (NMQR 3716) and *Thrinaxodon* (SAM-PK-K1395), *Thrinaxodon* had much thicker peripheral lamellar tissue. This suggests *Thrinaxodon* reached sexual maturity sooner than *Galesaurus* (Butler, 2009). Our observations that *Thrinaxodon* had an earlier (accelerated) ontogenetic development of the posterior sagittal crest (Table 5), and that *Galesaurus* reached the adult stage at a relatively larger skull size (BSL 90 mm), also indicate that *Galesaurus* reached sexual maturity relatively later than *Thrinaxodon*.

CONCLUSIONS

This comprehensive study of *Galesaurus* revealed several changes in morphology of the skull and mandible that occurred during ontogeny. Most of these changes developed during the transition between subadult and adult stages. For example, changes in structure of the zygomatic arch, development of the posterior sagittal crest, medial shift of the mandible within the temporal fenestra, and fusion of several occipital elements with the exoccipital, occurred during the transition to adulthood. These changes suggest that the masseter, temporalis, and nuchal musculature became much more developed in adult individuals of *Galesaurus*.

This is the first time sexual dimorphism has been documented in a basal epicynodont, with at least four cranial features dividing the adult sample of *Galesaurus* into two morphs. The most distinctive difference is the lateral flaring of the zygomatic arches in "males", which suggests an increased development of the masseter musculature and possibly bite force. In addition, the orbits are more anteriorly oriented, which is an indirect consequence of the flaring of the zygomatic arches, the snout width increased, and the relative length of the temporal region increased in the adult 'males' (Table 7). These differences between the two adult morphs reflect a difference in cranial function, which might be a result of dietary differences between the sexes or perhaps antagonistic behaviour in the "males".

A comparison of *Galesaurus* with *Thrinaxodon* revealed differences in cranial ontogeny and function between these two basal cynodonts. In *Galesaurus*, eight craniomandibular changes occurred during ontogeny separating the sample of thirty-one specimens into three ontogenetic stages. In contrast, nine cranial ontogenetic changes were documented in *Thrinaxodon*, dividing the much larger sample into four ontogenetic stages, including a division between the early and late juveniles (Jasinoski et al., 2015). Both taxa shared a few cranial ontogenetic features, but the degree and timing of two of these changes differed. For instance, the posterior sagittal crest developed much later at the adult stage in *Galesaurus*, whereas it formed at the late juvenile stage in *Thrinaxodon*. Other ontogenetic changes in *Galesaurus* such as the large shift

in the relative position of the mandible and partial fusion of the occiput were quite dramatic and not documented before in a basal cynodont. The ontogenetic changes and allometric trends in the zygomatic arch suggested that the masseter muscles in *Galesaurus* were more developed than in *Thrinaxodon*.

In summary, the combination of the two comprehensive ontogenetic surveys of the basal cynodonts *Galesaurus* and *Thrinaxodon* revealed that the development of the adductor musculature appears to have been one of the main factors influencing the growing skull.

ACKNOWLEDGEMENTS

The authors thank K. Carlson and K. Jakata (Evolutionary Studies Institute [ESI], University of the Witwatersrand) for micro-CT scanning *Galesaurus* specimens, as well as T. Nemavhundi (ESI), C. Dube (ESI), and the preparators at the Ditsong National Museum of Natural History and the National Museum for further preparation of fossil material. The following people are acknowledged for providing additional digital photographs of specimens of *Galesaurus*: J. Hopson, K. Angielczyk, E. Butler, C. Grau, B. McPhee, and P. Barrett. Also T. Jashashvili and D. Flores are thanked for assistance with the multivariate analysis. K. Angielczyk, J. Hopson, A. Crompton, E. Allin, Z-X. Luo, and an anonymous reviewer are thanked for their helpful discussions and comments.

LITERATURE CITED

Abdala F. 1996. Los chiniquodontoideos (Synapsida, Cynodontia) sudamericanos. South American Chiniquodontoids (Synapsida, Cynodontia). PhD thesis. Facultad de Ciencias Naturales, Universidad Nacional de Tucumán.

Abdala F. 2003. Galesaurid cynodonts from the Early Triassic of South Africa: another example of conflicting distribution of characters in non-mammalian cynodonts. South African J Sci 99: 95–96.

Abdala F. 2007. Redescription of *Platycraniellus elegans* (Therapsida, Cynodontia) from the lower Triassic of South Africa, and the cladistic relationships of eutheriodonts. Palaeontology 50: 591–618.

Abdala F, Damiani R. 2004. Early development of the mammalian superficial masseter muscle in cynodonts. Palaeontol Afr 40: 23–29.

Abdala F, Flores DA, Giannini NP. 2001. Postweaning ontogeny of the skull of *Didelphis albiventris*. J Mammal 82:190–200.

Abdala F, Giannini NP. 2000. Gomphodont cynodonts of the Chañares Formation: the analysis of an ontogenetic sequence. J Vertebr Paleontol 20:501–506.

Abdala F, Giannini NP. 2002. Chiniquodontid cynodonts: systematic and morphometric considerations. Palaeontology 45:1151–1170.

Abdala F, Jasinoski SC, Fernandez V. 2013. Ontogeny of the early triassic cynodont *Thrinaxodon liorhinus* (Therapsida): dental morphology and replacement. J Vertebr Paleontol 33:1408–1431.

Allin EF. 1975. Evolution of the mammalian middle ear. J Morphol 147:403–438.

Allin EF, Hopson JA. 1992. Evolution of the auditory system in Synapsida ("Mammal-like reptiles" and primitive mammals) as seen in the fossil record. In: Webster DB, Fay RR, Popper AN, editors. The evolutionary biology of hearing. New York: Springer-Verlag. p 587–614.

Ashton EH, Zuckerman S. 1956. Cranial crests in the anthropoidea. Proc Zool Soc Lond 126:581–634.

Barghusen HR. 1968. The lower jaw of cynodonts (Reptilia, Therapsida) and the evolutionary origin of mammal-like adductor jaw musculature. Postilla 116:1–49.

Boonstra LD. 1935. A note on the cynodont, *Glochinodontoides gracilis* Haughton. Am Mus Novitates 782:1–6.

Bradu D, Grine FE. 1979. Multivariate analysis of diademodontine crania from South Africa and Zambia. South Afr J Sci 75:441–448.

Brink AS. 1954a. Note on a new *Platycraniellus* skull. Navors Nas Mus Bloemfontein 1:127–129.

Brink AS. 1954b. *Thrinaxodon* and some other *Lystrosaurus* zone cynodonts in the collection of the National Museum, Bloemfontein. Navors Nas Mus Bloemfontein 1:115–125.

Brink AS. 1963. A new skull of the procynosuchid cynodont *Leavachia duvenhagei* Broom. Palaeontol Afr 8:57–75.

Brink AS. 1965. On two new specimens of *Lystrosaurus*-Zone cynodonts. Palaeontol Afr 9:107–122.

Brink AS, Kitching JW. 1951. Some theriodonts in the collection of the Bernard Price Institute. Ann Mag Nat Hist 72:1218–1236.

Broom R. 1932a. The cynodont genus *Galesaurus*. Ann Natal Mus 7:61–66.

Broom R. 1932b. The mammal-like reptiles of South Africa and the origin of mammals. London: H.F. & G. Witherby.

Broom R. 1936. On some new genera and species of Karroo fossil reptiles, with notes on some others. Ann Transvaal Mus 18: 349–386.

Broom R. 1938. On the structure of the skull of the cynodont, *Thrinaxodon liorhinus*, Seeley. Ann Transvaal Mus 19:263–269.

Butler E. 2009. The postcranial skeleton of the Early Triassic non-mammalian cynodont *Galesaurus planiceps*: implications for biology and lifestyle. M.Sc. thesis, University of the Free State.

Cartmill M. 1972. Arboreal adaptations and the origin of the order Primates. In: Tuttle R, editor. The functional and evolutionary biology of primates. Chicago: Aldine-Atherton. p 97–122.

Cox PG. 2008. A quantitative analysis of the Eutherian orbit: correlations with masticatory apparatus. Biol Rev 83:35–69.

Crompton AW. 1963. On the lower jaw of *Diarthrognathus* and the origin of the mammalian lower jaw. Proc Zool Soc Lond 140: 697–753.

Emerson S, Bramble D. 1993. Scaling, allometry, and skull design. In: Hanken J, Hall BK, editors. The skull, Vol. 3. Chicago: University of Chicago Press. p 384–421.

Flores DA, Abdala F, Giannini N. 2010. Cranial ontogeny of *Caluromys philander* (Didelphidae: Caluromyinae): a qualitative and quantitative approach. J Mammal 91:539–550.

Flores DA, Abdala F, Giannini NP. 2013. Post-weaning cranial ontogeny in two bandicoots (Mammalia, Peramelomorphia, Peramelidae) and comparison with carnivorous marsupials. Zoology 116:372–384.

Fourie S. 1974. The cranial morphology of *Thrinaxodon liorhinus* Seeley. Ann South Afr Mus 65:337–400.

Garcia-Perea R. 1996. Patterns of postnatal development in skulls of lynxes, genus *Lynx* (Mammalia: Carnivora). J Morphol 229: 241–254.

Giannini NP, Abdala F, Flores DA. 2004. Comparative postnatal ontogeny of the skull of *Dromiciops gliroides* (Marsupialia: Microbiotheriidae). Am Mus Novitates 3460:1–17.

Grine FE, Hahn BD. 1978. Allometric growth in the Diademodontinae (Reptilia; Therapsida): a preliminary report. Palaeontol Afr 21:161–166.

Grine FE, Hahn BD, Gow CE. 1978. Aspects of relative growth and variability in *Diademodon* (Reptilia; Therapsida). South African J Sci 74:50–58.

Hammer Ø. 2015. PAST, Palaeontological Statistics. Version 3.10. Reference Manual.

Hammer Ø, Harper DAT, Ryan PD. 2001. PAST: paleontological statistics software package for education and data analysis. Palaeontol Electron 4:1–9.

Haughton SH. 1924. On Cynodontia from the Middle Beaufort beds of Harrismith, Orange Free State. Ann Transvaal Mus 11:74–92.

Haughton SH, Brink AS. 1954. A bibliographic list of Reptilia from the Karoo beds of Africa. Palaeontol Afr 2:1–171.

Heesy CP. 2004. On the relationship between orbit orientation and binocular visual field overlap in mammals. Anat Rec 281A:1104–1110.

Heesy CP. 2008. Ecomorphology of orbit orientation and the adaptive significance of binocular vision in primates and other mammals. Brain Behav Evol 71:54–67.
Herrel A, van Damme R, de Vree F. 1996. Sexual dimorphism of head size in *Podarcis hispanica atrata*: testing the dietary divergence hypothesis by bite force analysis. Neth J Zool 46:253–262.
Hopson JA, Barghusen HR. 1986. An analysis of therapsid relationships. In: Hotton N, MacLean PD, Roth JJ, Roth EC, editors. The ecology and biology of mammal-like reptiles. Washington: Smithsonian Institutional Press. p 83–106.
Hopson JA, Kitching JW. 1972. A revised classification of cynodonts (Reptilia; Therapsida). Palaeontol Afr 14:71–85.
Hopson JA, Kitching JW. 2001. A probainognathian cynodont from South Africa and the phylogeny of non-mammalian cynodonts. Bull Mus Comp Zool 156:5–35.
Iordansky N. 1970. Structure and biomechanical analysis of functions of the jaw muscles in lizards. Anat Anz 127:383–413.
Jasinoski SC, Abdala F, Fernandez V. 2015. Ontogeny of the Early Triassic cynodont *Thrinaxodon liorhinus* (Therapsida): cranial morphology. Anat Rec 298:1440–1464.
Kammerer CF, Flynn JJ, Ranivoharimanana L, Wyss AR. 2012. Ontogeny in the Malagasy traversodontid *Dadadon isaloi* and a reconsideration of its phylogenetic relationships. Fieldiana Life Earth Sci 5:112–125.
Kermack KA, Mussett F, Rigney HW. 1981. The skull of *Morganucodon*. Zool J Linn Soc 71:1–158.
Kielan-Jaworowska Z, Cifelli RL, Luo Z-X. 2004. Mammals from the age of dinosaurs: origins, evolution, and structure. New York: Columbia University Press.
Köhler M, Moyà-Solà S. 2004. Reduction of brain and sense organs in the fossil insular bovid *Myotragus*. Brain Behav Evol 63: 125–140.
Kühne WG. 1956. The Liassic therapsid *Oligokyphus*. London: British Museum (Natural History).
Meachen-Samuels J, Van Valkenburgh B. 2009. Craniodental indicators of prey size preference in the Felidae. Biol J Linn Soc 96: 784–799.
Mitchell G, Roberts DG, van Sittert SJ, Skinner JD. 2013. Orbit orientation and eye morphometrics in giraffes (*Giraffa camelopardalis*). Afr Zool 48:333–339.
Mosimann JE, James FC. 1979. New statistical methods for allometry with application to Florida red-winged blackbirds. Evolution 33:444–459.
Noble VE, Kowalski EM, Ravosa MJ. 2000. Orbit orientation and the function of the mammalian postorbital bar. J Zool (Lond) 250: 405–418.
Olson EC. 1944. Origin of mammals based upon cranial morphology of the therapsid suborders. Geol Soc Am Special Paper 55:1–130.
Onar V, Pazvant G, Ince NG, Alpak H, Janeczek M, Kiziltan Z. 2013. Morphometric analysis of the foramen magnum of byzantine dogs excavated in Istanbul Yenikapi at the site of Theodosius harbour. Mediterr Archaeol Archaeometry 13:135–142.
Owen R. 1859. On some reptilian remains from South Africa. Edinb New Philos J 10:289–291.
Owen R. 1860. On some reptilian fossils from South Africa. Q J Geol Soc Lond 16:49–63.
Owen R. 1876. Descriptive and illustrated catalogue of the fossil Reptilia of South Africa in the collection of the British Museum. British Museum (Natural History), London.
Parrington FR. 1934. On the cynodont genus *Galesaurus*, with a note on the functional significance of the changes in the evolution of the theriodont skull. Ann Mag Nat History 13:38–67.
Rager L, Hautier L, Forasiepi A, Goswami A, Sánchez-Villagra MR. 2014. Timing of cranial suture closure in placental mammals: phylogenetic patterns, intraspecific variation, and comparison with marsupials. J Morphol 275:125–140.
Rigney HW. 1938. The morphology of the skull of a young *Galesaurus planiceps* and related forms. J Morphol 63:491–529.
Romer AS. 1970. The Chañares (Argentina) Triassic reptile fauna. VI. A chiniquodontid cynodont with an incipient squamosal-dentary jaw articulation. Breviora 344:1–18.
Rowe T, Carlson W, Bottorff W. 1995. *Thrinaxodon*: digital atlas of the skull. CD-ROM, (2nd ed., for Windows and Macintosh platforms), University of Texas Press, 547 megabytes.
Sánchez-Villagra MR. 2010. Suture closure as a paradigm to study late growth in recent and fossil mammals: a case study with giant deer and dwarf deer skulls. J Vertebr Paleontol 30:1–4.
Shine R. 1989. Ecological causes for the evolution of sexual dimorphism: a review of the evidence. Q Rev Biol 64:419–461.
Sidor CA, Smith RMH. 2004. A new galesaurid (Therapsida: Cynodontia) from the Lower Triassic of South Africa. Palaeontology 47: 535–556.
Simpson GG, Roe A, Lewontin RC. 2003. Quantitative zoology, revised edition. Mineola: Dover Publications.
Smith R, Botha J. 2005. The recovery of terrestrial vertebrate diversity in the South African Karoo Basin after the end-Permian extinction. Comptes Rendus Palevol 4:623–636.
Smith RMH, Botha-Brink J. 2014. Anatomy of a mass extinction: sedimentological and taphonomic evidence for drought-induced die-offs at the Permo-Triassic boundary in the main Karoo Basin, South Africa. Palaeogeogr Palaeoclimatol Palaeoecol 396:99–118.
Smith R, Rubidge B, van der Walt M. 2012. Therapsid biodiversity patterns and paleoenvironments of the Karoo Basin, South Africa. In: Chinsamy-Turan A, editor. Forerunners of mammals, radiation, histology, biology. Bloomington: Indiana University Press. p 31–62.
Tatarinov LP. 1968. Morphology and systematics of the Northern Dvina cynodonts (Reptilia, Therapsida; Upper Permian). Postilla 126:1–51.
Teixeira AMS. 1982. Um novo cinodonte carnívoro (*Probelesodon kitchingi* sp. nov.) do Triássico do Rio Grande do Sul, Brasil. Comunicaoções do Museu de Ciências da PUCRGS 24:1–31.
Turnbull W. 1970. Mammalian masticatory apparatus. Fieldiana Geol 18:149–356.
Van den Brandt MJ. 2013. Cranial morphology and phylogenetic analysis of *Cynosaurus suppostus* (Therapsida, Cynodontia) from the Upper Permian of the Karoo Basin, South Africa. Honours Thesis. Evolutionary Studies Institute, University of the Witwatersrand.
van Heerden J. 1972. Interspecific variation and growth changes in the cynodont reptile *Thrinaxodon liorhinus*. Navors Nas Mus Bloemfontein 2:307–347.
van Hoepen ECN. 1916. Preliminary notice of some new reptiles of the Karroo Formation. Ann Transvaal Mus 5:1–2.
Vincent SE, Herrel A. 2006. Functional and ecological correlates of ecologically-based dimorphisms in squamate reptiles. Integr Comp Biol 47:172–188.
Watson AG, de Lahunta A, Evans HE. 1989. Dorsal notch of foramen magnum due to incomplete ossification of supraoccipital bone in dogs. J Small Anim Pract 30:666–673.
Watson DMS. 1920. On the Cynodontia. Ann Mag Nat Hist 6: 506–524.
Werneburg I. 2011. The cranial musculature of turtles. Palaeontol Electron 14:1–99.